ARTICLE

Unveiling skin macrophage dynamics explains both tattoo persistence and strenuous removal

Anna Baranska[1] , Alaa Shawket[1]*, Mabel Jouve[3]*, Myriam Baratin[1]* , Camille Malosse[1], Odessa Voluzan[1], Thien-Phong Vu Manh[1], Frédéric Fiore[2] , Marc Bajénoff[1], Philippe Benaroch[4], Marc Dalod[1], Marie Malissen[1,2] , Sandrine Henri[1]**, and Bernard Malissen[1,2]**

Here we describe a new mouse model that exploits the pattern of expression of the high-affinity IgG receptor (CD64) and allows diphtheria toxin (DT)–mediated ablation of tissue-resident macrophages and monocyte-derived cells. We found that the myeloid cells of the ear skin dermis are dominated by DT-sensitive, melanin-laden cells that have been missed in previous studies and correspond to macrophages that have ingested melanosomes from neighboring melanocytes. Those cells have been referred to as melanophages in humans. We also identified melanophages in melanocytic melanoma. Benefiting of our knowledge on melanophage dynamics, we determined the identity, origin, and dynamics of the skin myeloid cells that capture and retain tattoo pigment particles. We showed that they are exclusively made of dermal macrophages. Using the possibility to delete them, we further demonstrated that tattoo pigment particles can undergo successive cycles of capture–release–recapture without any tattoo vanishing. Therefore, congruent with dermal macrophage dynamics, long-term tattoo persistence likely relies on macrophage renewal rather than on macrophage longevity.

Introduction

Recent studies, based on ontogeny and transcriptomic analysis, have succeeded in discriminating conventional dendritic cells (cDCs) from monocyte-derived cells. cDCs comprise two lineages known as cDC1 and cDC2 (Guilliams et al., 2016), have a short life span, and are continually replenished from committed cDC precursors that originate in the bone marrow (BM). Under steady-state conditions, BM-derived blood Ly-6C^{high} monocytes extravasate at a slow pace into nonlymphoid tissues, such as the intestinal lamina propria and the skin dermis, where they give rise to two developmental streams (Tamoutounour et al., 2012, 2013; Bain et al., 2013; Jakubzick et al., 2013). Progression through the first developmental stream is associated with the preservation of CC-chemokine receptor 2 (CCR2) expression, the acquisition of MHCII molecules, and a diminution of Ly-6C expression. It can be visualized in Ly-6C–MHCII dot plots as a "monocyte waterfall," the final product of which share features with cDC2 and is called monocyte-derived DC (mo-DCs; Tamoutounour et al., 2013). Blood Ly-6C^{hi} monocytes extravasate at a higher pace into inflamed tissues (Tamoutounour et al., 2012, 2013; Bain et al., 2013) and give rise to cells that, because of their ability to produce TNFα and inducible NO synthase, are denoted as Tip-DCs (Serbina et al., 2003; De Trez et al., 2009; Tamoutounour et al., 2012). Under steady-state conditions, extravasated Ly-6C^{high}

monocytes also proceed through a second developmental stream yielding tissue-resident macrophages (mo-Mac) that have lost expression of CCR2 and Ly-6C and express or not MHCII molecules (Jakubzick et al., 2013; Tamoutounour et al., 2013; Yona et al., 2013; Bain et al., 2014; McGovern et al., 2014). In the intestine and dermis, such mo-Mac replace in part or in totality a pool of macrophages that develops before the establishment of definitive hematopoiesis in a CCR2-independent manner (Tamoutounour et al., 2013; Bain et al., 2014; Sheng et al., 2015). Monocyte fate toward mo-Mac or mo-DCs is specified by microenvironmental cues (Goudot et al., 2017).

The possibility of discriminating cDCs from mo-DCs and macrophages emphasized their distinct functional specialization. Upon infection, antigen-laden cDCs migrate to draining LNs and trigger the conversion of antigen-specific naive T cells into effector T cells. In contrast, most mo-DCs remain in tissue parenchyma where they contribute to local immune responses and provide potent antimicrobial function during infection. Macrophages contribute to tissue homeostasis and wound repair because of their capacity to phagocyte cellular debris, invading organisms, and apoptotic cells. Owing to their strategic positioning at body barriers, macrophages capture a wide range of exogenous particulates. They also ingest self-derived particulates, as
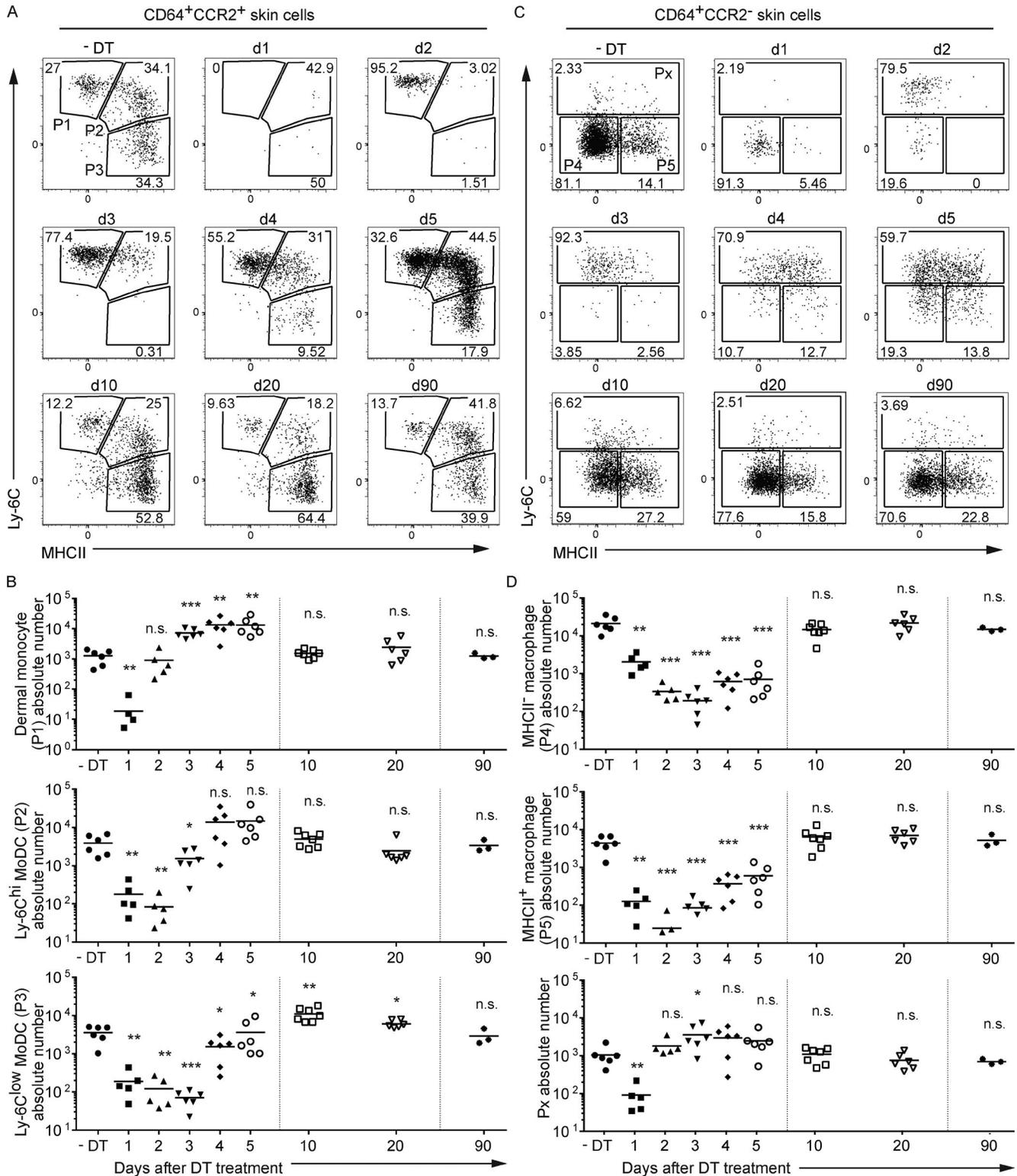
Figure 1. **Replenishment kinetics of monocytes, mo-DCs, and macrophages in the dermis of CD64^{dtr} mice after DT treatment.** CD64^{dtr} mice were left untreated (-DT) or treated twice and 24 h apart with DT. Analysis of the CD64$^+$CCR2$^+$monocytes and mo-DCs and CD64$^+$CCR2$^-$ macrophages found in the ear dermis (Fig. S1 A) was performed before (-DT) and 1, 2, 3, 4, 5, 10, 20, and 90 d after the last DT injection. **(A)** CD64$^+$CCR2$^+$ dermal cells were analyzed at the specified time points by using Ly-6C–MHCII dot plots to define the percentages of Ly-6C$^+$MHCII$^-$ (P1) dermal monocytes, Ly-6C$^+$MHCII$^+$ (P2) mo-DCs, and Ly-6C$^-$MHCII$^+$ (P3) mo-DCs (Tamoutounour et al., 2013). **(B)** Quantification of the results in A showing the absolute number of cells obtained from two ears of each mouse. Each symbol corresponds to a mouse and the mean (horizontal bar) is indicated. **(C)** CD64$^+$CCR2$^-$ dermal cells were analyzed at the specified time points by using Ly-6C–MHCII dot plots to define the percentages of Ly-6C$^-$MHCII$^-$ (P4) dermal macrophages and Ly-6C$^-$MHCII$^+$ (P5) dermal macrophages (Tamoutounour et al., 2013). A Ly-6C$^+$MHCII$^{-\ to\ high}$ cell population transiently developed 2–5 d after the last DT treatment and is denoted as Px cells. **(D)**

exemplified by the melanin-laden macrophages that have been sporadically observed in the normal human dermis and referred to as "melanophages" (Haniffa et al., 2009, 2012).

To study the functional specialization that exists among cells of the mononuclear phagocyte system, several strains of gene-targeted mice have been developed to ablate a given cell subset by placing the human diphtheria toxin receptor (hDTR) under the control of a gene promoter specific for the subset of interest. Those models are sometimes associated with drawbacks (van Blijswijk et al., 2015; Durai and Murphy, 2016). For instance, in CD11b-DTR mice, cDC2s, macrophages, and mo-DCs were depleted, and because of off-target DTR expression, those mice died after a few diphtheria toxin (DT) injections (Duffield et al., 2005). Although CCR2-DTR mice were not prone to DT-induced lethality (Hohl et al., 2009), some of the phenotypes observed by using those mice likely resulted from the depletion of CCR2+ cDC2s rather than of monocytes and monocyte-derived cells as generally assumed (Malissen et al., 2014).

In contrast to cDCs, both the mo-DCs and mo-Mac, including their precursors, and the macrophages of embryonic origin that are found in tissues such as the skin, the lung, and the gut express the high-affinity IgG receptor FcgRI (CD64; Bain et al., 2013; Plantinga et al., 2013; Tamoutounour et al., 2013). Here, we developed mice in which a hDTR gene was placed under the control of the *Fcgr1* gene that codes for CD64. This model has a tighter ablation specificity compared with previous models in that it permitted specifically ablating macrophages, monocytes, and monocyte-derived cells in vivo. It allowed us to identify in the ear skin dermis of C57BL/6 (B6) mice a population of melanophages that constitutes a quantitatively major subset of dermal myeloid cells and has been missed in previous studies. By characterizing their phenotype, origin, and dynamics, we showed that they corresponded to dermal macrophages that have ingested melanin granules. Benefiting from the knowledge gained on melanophage dynamics, we further elucidated the identity, origin, and dynamics of the myeloid cells that are found in the mouse skin and capable of capturing and retaining tattoo pigment particles.

Results

Mice permitting ablation of macrophages and monocyte-derived cells

To assess the dynamics and functional role of CD64+ macrophages and monocyte-derived cells in vivo, we generated a line of gene-targeted mice containing in the 3′-UTR of the *Fcgr1* gene a cassette composed of an internal ribosomal entry site, an enhanced green fluorescent protein (EGFP), a 2A cleavage sequence, and an hDTR. To demonstrate that the mo-Mac and monocyte-derived cells found in mice homozygous for the *Fcgr1-IRES-EGFP-hDTR* allele (also known as *B6-Fcgr1^{tm1Ciphe}* and called CD64^{dtr} mice here) developed normally and expressed normal

levels of CD64, we analyzed their skin dermis because it contains a full complement of such cells (Fig. S1 A; Tamoutounour et al., 2013). Among dermal CD11b+ cells, cDC2s can be distinguished from non-cDC2s cells by their Ly-6C−CD64− phenotype. Dermal CD11b+CD64+ non-cDC2 cells can be further resolved into CCR2+ and CCR2− cells. CCR2+ cells comprise Ly-6C^{high}MHCII− dermal monocytes (P1), Ly-6C^{high} (P2), and Ly-6C− (P3) MHCII+ mo-DCs that constitute a P1 → P2 → P3 developmental series. CCR2− cells comprise MHCII^{low} (P4) and MHCII^{high} (P5) dermal macrophages. The ear skin dermis of DT-untreated CD64^{dtr} mice showed ratios and numbers of monocytes, mo-DCs, and macrophages comparable to those of WT mice (Fig. S1 B), and all those cells expressed normal levels of CD64 (Fig. S1 C). Similar results were obtained when CD64+ cells found in the lamina propria of the large intestine were analyzed (not depicted).

CD64^{dtr} mice were treated with DT twice and 24 h apart without lethality, and the myeloid cells present in the ear skin were analyzed at various time points after the last DT injection. DT treatment was not associated with overt inflammation as documented by the lack of skin infiltrating neutrophils (not depicted). CD64+CCR2+ cells were all ablated within 24 h (Fig. 1, A and B), demonstrating that the hDTR was functional. 48 h after the last DT injection, Ly-6C^{high}MHCII− dermal monocytes started to return, and Ly-6C^{high} and Ly-6C− MHCII+ mo-DCs were replenished in sequence over the next 5 d. A transient rebound in their numbers occurred around day 4, suggesting that their rate of generation can increase in response to acute, DT-induced loss. Both MHCII^{low} and MHCII^{high} CCR2−CD64+ dermal macrophages showed protracted reconstitution kinetics compared with CD64+CCR2+ cells in that it took up to 10 d to fully reconstitute their pools (Fig. 1, C and D). Analysis of the gate corresponding to CCR2−CD64+ cells at days 2–3 revealed a population of Ly-6C^{high}MHCII^{low to high} cells (denoted as Px cells in Fig. 1, C and D) that started losing Ly-6C expression on day 4 and thus progressively merged within gates corresponding to MHCII^{low} and MHCII^{high} dermal macrophages. The phenotype, kinetics of reappearance of Px cells, and the occurrence at days 4 and 5 of cells straddling the Px and P4/P5 gates suggest that they correspond to intermediaries between Ly-6C^{high} blood monocytes and MHCII^{low} and MHCII^{high} dermal macrophages. The percentage of Px cells among CCR2−CD64+ cells reached pre-DT-treatment levels upon replenishment of the MHCII^{low} and MHCII^{high} dermal macrophage compartments (Fig. 1, C and D).

In the lamina propria of the large intestine of CD64^{dtr} mice, CD64+ cells were also ablated within 24 h after the last DT injection and reconstituted from 48 h onward akin to dermal CD64+ cells (Fig. S2). Therefore, by allowing to conditionally empty the niche occupied in the skin dermis and intestinal lamina propria by CD64+ myeloid cells, the CD64^{dtr} mouse model demonstrated that all the mo-DC and macrophage subsets that were present in adult skin and intestine before DT treatment can be readily

---
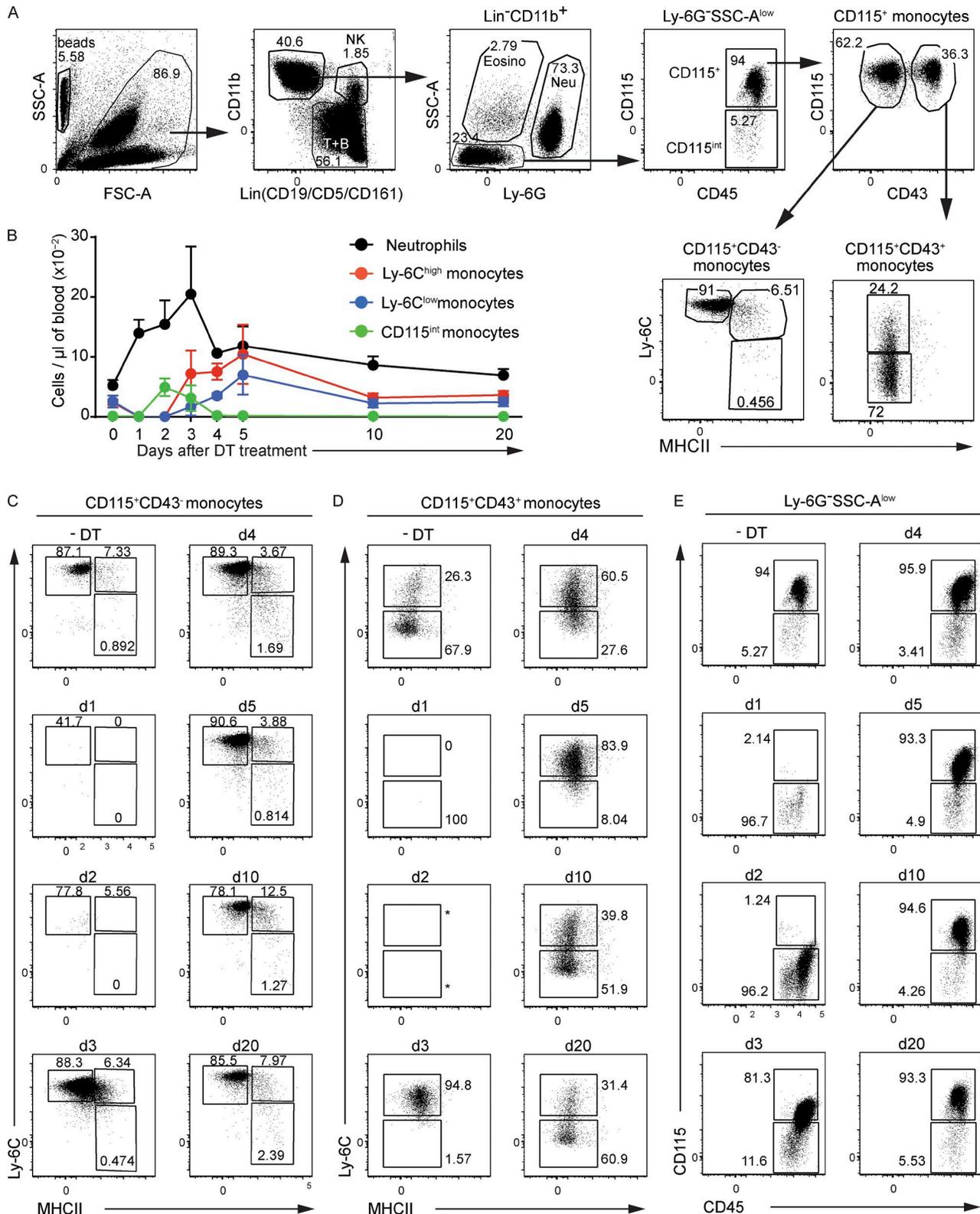
Figure 2. **Replenishment kinetics of blood monocytes of CD64^dtr mice after DT treatment. (A)** Gating strategy used to identify CD11b⁺Lin⁻ cell subsets within the blood. Red blood cells were lysed before analysis, and the absolute number of a given cell type present in a given blood volume was determined by staining samples in Trucount Absolute Counting Tubes. Beads were gated out on the basis of their FSC-A–SSC-A profile, and after excluding CD5⁺ T cells, CD19⁺ B cells, CD161⁺ NK cells, as well as SSC-A^int eosinophils, and Ly-6G⁺ neutrophils, the majority of the remaining CD11b⁺Lin⁻ cells were CD45⁺CD115⁺; when analyzed on CD115-CD43 dot plots, they comprise CD115⁺CD43⁻ and CD115⁺CD43⁺ subsets. As expected, CD115⁺CD43⁻ cells corresponded to Ly-6C^high blood monocytes, whereas most CD115⁺CD43⁺ corresponded to Ly6-C^low blood monocytes. **(B)** Absolute number (mean values ± SD) of the specified cells in the

reconstituted in normal ratios and numbers and with kinetics consistent with their expected precursor–product relationship.

Kinetics of replenishment of blood monocytes after DT treatment

Adult steady-state monopoiesis occurs in BM, where monocyte–macrophage DC progenitors (MDPs) give rise to common monocyte progenitors (cMoP) that generate two main blood monocyte subsets that are both CD115 (CSF1R)$^+$ and can be distinguished on the basis of CD43 expression (Fig. 2 A). CD43$^-$ cells are CX3CR1^{int}CCR2$^+$CD64$^+$Ly-6C^{high} and CD43$^+$ cells are mostly CX3CR1^{high}CCR2$^-$CD64$^+$Ly-6C^{low} (Sunderkötter et al., 2004). They are denoted here as Ly-6C^{high} and Ly-6C^{low} monocytes, respectively. Ly-6C^{low} monocytes remain within blood vessels (Carlin et al., 2013) whereas Ly-6C^{high} monocytes contribute to the replenishment of mo-DCs and mo-Mac in tissues, including the skin and the intestine (Jakubzick et al., 2013; Tamoutounour et al., 2013; Yona et al., 2013; Bain et al., 2014; McGovern et al., 2014). Intraperitoneal injection of DT twice and 24 h apart resulted within 24 h in the complete ablation of the MDPs and cMoPs and Ly-6C^{high}, Ly-6C^{int}, and Ly-6C^{low} monocytes found in the BM (Fig. S3) and of the Ly-6C^{high} and Ly-6C^{low} blood monocytes (Fig. 2, B–D). Analysis of the blood and BM of CD64^{dtr} mice at various time points after the last DT injection showed that blood Ly-6C^{high} and Ly-6C^{low} monocytes were rapidly replenished and that a transient rebound in their numbers occurred (Fig. 2, B–D; and Fig. S3). Consistent with the observation that CD115 is dramatically down-regulated in response to CSF-1 (Yu et al., 2012), the earliest BM-derived monocytes reappearing in the blood expressed lower levels of CD115 than CD115$^+$ steady-state monocytes and are denoted here as CD115^{int} cells (Fig. 2, A, B, and E). Because of their CD115^{int} phenotype, those Ly-6C^{high} monocytes were not recorded in the CD115$^+$CD43$^-$ gate used in Fig. 2 C. Their numbers peaked at day 3 after DT treatment (Fig. 2, B and E), and when blood monocytes were fully replenished, their relative representation dramatically decreased. Congruent with the view that circulating CD43$^-$Ly-6C^{high} monocytes give rise to CD43$^+$ Ly-6C^{low} monocytes (Varol et al., 2007; Thomas et al., 2016; Mildner et al., 2017), the first CD43$^+$ monocytes reappeared at days 3–4 after the last DT treatment and gradually lost Ly-6C expression (Fig. 2 D). An approximately fourfold increase in blood neutrophils occurred in CD64^{dtr} mice and peaked 3 d after DT treatment (Fig. 2 B). It occurred, however, with a far lower magnitude and shorter duration than that observed upon DT administration in CD11c-DTR mice (Autenrieth et al., 2012; Tittel et al., 2012).

DT treatment of CD64^{dtr} mice spares skin cDCs

We analyzed next whether DT treatment of CD64^{dtr} mice affects the cDCs found in the skin. Langerhans cells (LCs; CD24^{hi}CD11b$^+$),

cDC1s (CD11b$^-$CD24$^+$), cDC2s (CD24^{low}CD11b$^+$), and double-negative (DN) cDCs (CD11b$^-$CD24$^-$) were identified as described in Fig. S4 A. Although the absolute numbers of LCs, cDC1s, and DN cells were not affected by DT treatment, a 1.3-fold reduction in cDC2 absolute number was observed 1 d after DT treatment (Fig. S4 B). Therefore, our regimen of DT administration had a rather minimal impact on the cDC subsets found in the skin of CD64^{dtr} mice. CD64^{dtr} mice can thus be used to monitor the dynamics and function of macrophages and monocyte-derived cells without major collateral effects or lethality.

Melanophages predominate among dermal myeloid cells of B6 ear skin

Former analyses of CD45$^+$Lin$^-$ myeloid cells present in the ear skin dermis focused on SSC-A^{low}FSC-A$^{low\ to\ high}$ (SSC-A^{low} in short) cells, leaving aside an uncharacterized population of SSC-A^{high}FSC-A$^{low\ to\ int}$ (SSC-A^{high} in short) cells (Tamoutounour et al., 2013). After treatment of CD64^{dtr} mice with DT twice and 24 h apart, all those SSC-A^{high} cells were unexpectedly ablated (Fig. 3 A). Further characterization of such DT-sensitive, SSC-A^{high} cells showed that they had a CD24^{low}CD11b$^+$CD64$^+$CCR2$^-$ MHCII$^{+\ or\ -}$ phenotype identical to that of SSC-A^{low} dermal macrophages and that CD64 expression accounted for their DT sensitivity (Fig. 3 B).

In the almost hairless skin of mouse ears, melanocytes are primarily found in the dermis (Fig. 3 C; Aoki et al., 2009) and synthetize melanin pigment within specialized lysosome-related structures known as melanosomes. Considering that the SSC-A parameter used in cytometry is proportional to cell granularity and that CD64^{dtr} mice were of B6 origin and have a black coat, we surmised that the high granularity of the SSC-A^{high} myeloid cells found in the ear dermis was due to their capture of melanin granules from neighboring melanocytes. Hematoxylin and eosin staining of cytospin preparations showed that the SSC-A^{low}CCR2$^-$ CD64$^+$ cells and the SSC-A^{high} cells sorted from the ear dermis have typical features of tissue macrophages; they were large with prominent cytoplasmic vacuoles (Fig. 3 D). The vacuoles of SSC-A^{high} cells differed, however, from those of SSC-A^{low} CCR2$^-$ CD64$^+$ cells in that they were loaded with dark material (Fig. 3 D). Upon analysis by electron microscopy, such dark vacuolar material had an extremely electron-dense appearance and an ellipsoidal shape (~0.2 μm × 0.7 μm), two hallmarks of melanosomes (Fig. 3 E). All the ingested melanosomes were in a mature stage, showing a uniformly electron-dense granule without discernable internal structure (Fig. 3 E).

In contrast to their precursors, dermal macrophages do not express CX3CR1 (Tamoutounour et al., 2012). Consistent with our hypothesis that melanophages correspond to macrophages that ingested melanosomes, they were CX3CR1$^-$ (not depicted)

---

blood of CD64^{dtr} mice before and 1, 2, 3, 4, 5, 10, and 20 d after DT treatment. **(C)** CD115$^+$CD43$^-$ monocytes were analyzed at the specified time points by using Ly-6C–MHCII dot plots to define the percentages of Ly-6C^{high}MHCII$^-$ and Ly-6C^{high}MHCII$^+$ monocytes. **(D)** CD115$^+$CD43$^+$ cells were analyzed at the specified time points by using Ly-6C–MHCII dot plots to define the percentages of Ly-6C$^+$MHCII$^-$ and Ly-6C^{low}MHCII$^-$ monocytes. **(E)** Ly-6G$^-$SSC-A^{low} cells were analyzed at the specified time points by using CD115-CD45 dot plots to define the percentages of CD115^{int} and CD115$^+$ blood monocytes. Data are representative of at least three experiments involving three to six animals per group.
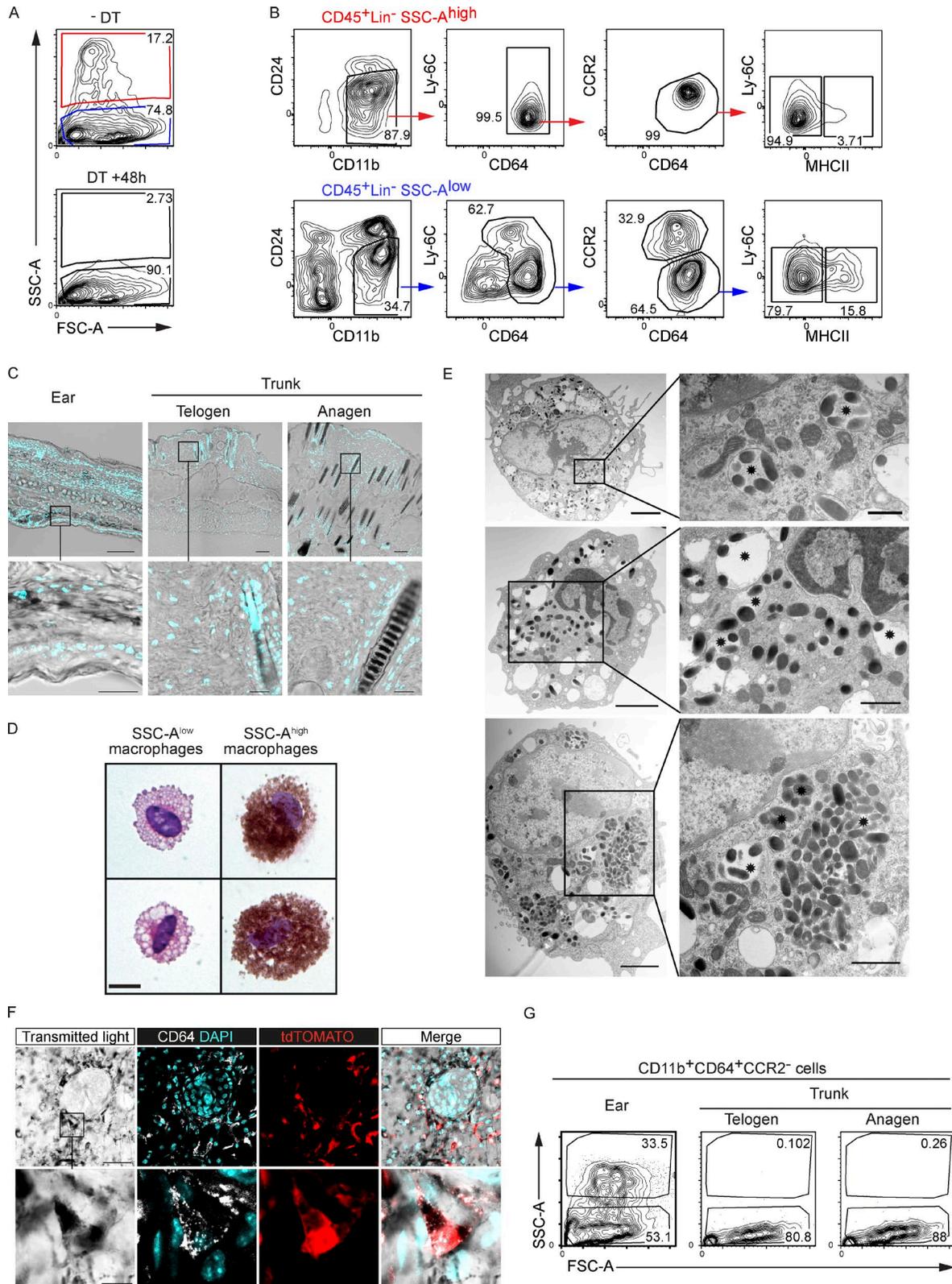
Figure 3. **CD64[dtr] mice unveil the existence of a novel CD64^{+} cell population in the skin that is highly granular and DT sensitive and corresponds to melanophages. (A)** Cell suspensions from the ear skin of CD64[dtr] mice were analyzed by flow cytometry before (-DT) or 48 h after (DT + 48 h) DT treatment. After excluding CD3^{+} T cells, CD19^{+} B cells, CD161^{+} NK cells, and Ly-6G^{+} neutrophils, the remaining lineage-negative (Lin^{−}) CD45^{+} live cells were analyzed by using FSC-A–SSC-A dot plots to define the percentages of SSC-A^{low} and SSC-A^{high} cells. **(B)** Comparative analysis of the SSC-A^{low} and SSC-A^{high} cells found in the ear skin by using a gating strategy resolving the cDC2s, monocytes, mo-DCs and macrophages present among CD45^{+}Lin^{−}CD11b^{+} cells (Fig. S1 A). The percentage of cells found in each of the specified gate is indicated. **(C)** Transversal tissue sections of B6 ear or trunk skin (at telogen and anagen phases) were stained with

and identified as melanin+tdTomato+CD64+ cells in the ear section of CX3CR1Cre/+ *Rosa*lsl-tdt/+ mice that fate map cells that have expressed CX3CR1 during their development (Fig. 3 F). In the densely haired mouse trunk, melanocytes are absent from the dermis and confined to the hair follicles where melanosomes are transferred from melanocytes to matrix keratinocytes to give rise to melanized hairs (Fig. 3 C). Such transfer is strictly coupled to the anagen phase of hair growth, and melanin is not formed during the telogen phase (Fig. 3 C; Slominski et al., 2005). Consistent with these anatomical features, the CD11b+CD64+CCR2- macrophages isolated from the trunk skin during both the anagen and telogen phases lacked melanophages (Fig. 3 G). Likewise, the ear skin of B6-albino and BALB/c mice, which is deprived of melanic pigment, also lacked SSC-Ahigh melanophages (Fig. 4, A and B). Therefore, the presence of dermal melanophages correlates with the presence of dermal melanocytes. Although they represent 55 ± 10% of the monocyte-derived cells present in the B6 ear dermis (Fig. 4, A and B), it is likely that melanophages have been missed in previous studies because of their unusual SSC-Ahigh phenotype.

Dynamics and origin of dermal melanophages

To assess the dynamics of dermal melanophages replenishment after DT-induced depletion, CD64dtr mice were treated with DT twice and 24 h apart. Melanophages were all ablated within 24 h, and their numbers fully reconstituted ∼20 d after the last DT injection (Fig. 5, A and B). The granularity of SSC-Ahigh cells, a proxy for melanin content, increased with time. The upper section (>190 K) of the SSC-Ahigh gate was only filled between days 20 and 90 after DT treatment, and a melanin content distribution identical to pre-DT-treatment levels was regained 90 d after DT treatment (Fig. 5, A and B). Although the dermis of CCR2-deficient mice is only populated by macrophages of prenatal origin that self-maintain without any input from adult monopoiesis (Tamoutounour et al., 2013), it showed a melanophage to macrophage ratio and melanin content distribution identical to that of WT dermis (Fig. 6 A). Therefore, the macrophages found in the ear dermis have the same propensity to capture melanin regardless of their prenatal (Fig. 6 A) or adult (Fig. 5) origin.
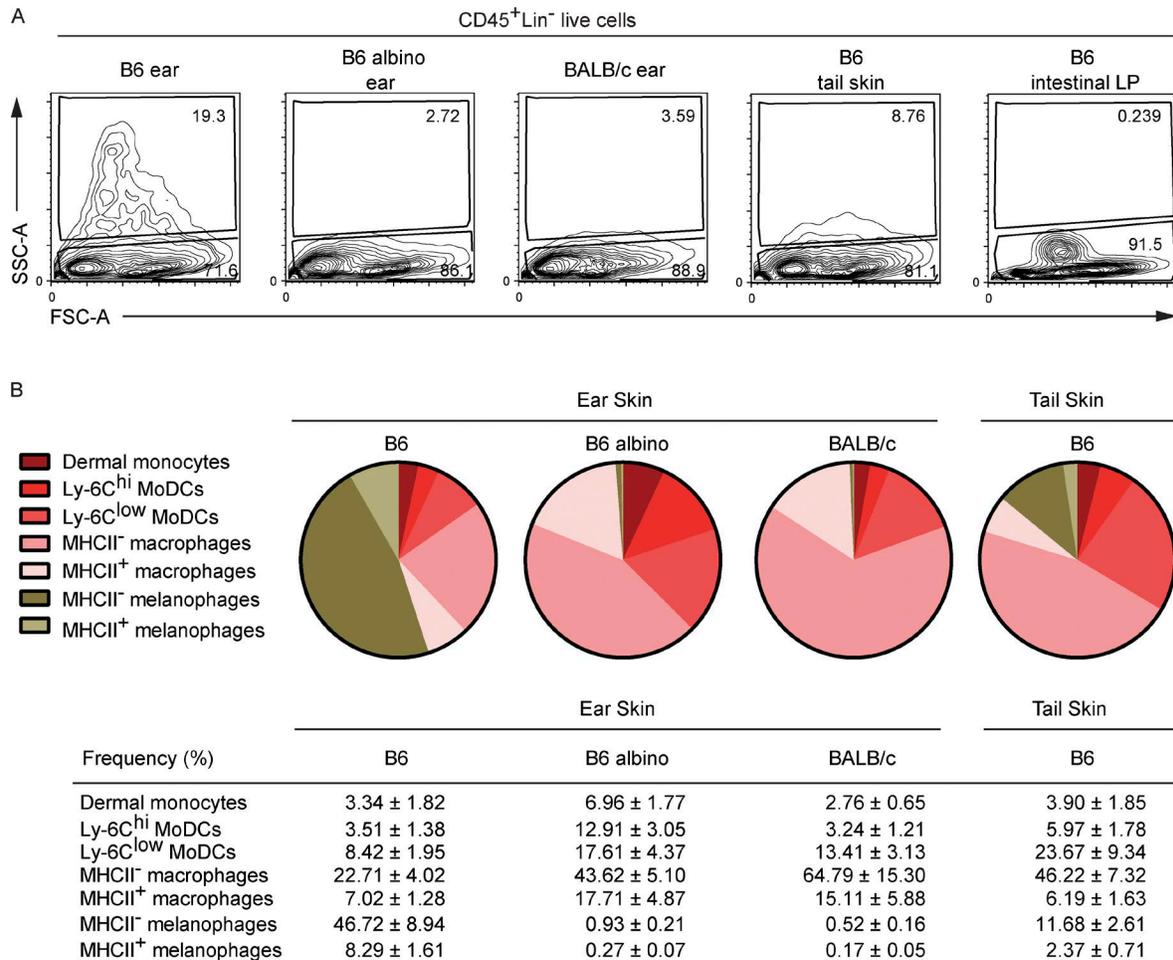
To demonstrate without relying on DT ablation that replenishment of the pool of adult dermal macrophages and melanophages relied on continuous input from BM-derived circulating precursors, parabiosis was established between adult mice expressing CD45.1 and CD45.2 (Fig. 6 B). Blood monocytes were allowed to exchange between parabionts for 8 wk before

assessing the presence of donor-derived macrophages and melanophages in the ear skin of each parabiont. Dermal MHC II+ macrophages contained ∼15% of cells originating from the parabiotic partner (Fig. 6 B), a distribution comparable to that of Ly-6Chigh blood monocytes and demonstrating that they continuously develop from BM monocytes (Tamoutounour et al., 2013; Sheng et al., 2015). Consistent with the view that a fraction of dermal MHCII- macrophages is of embryonic origin and self-renews in situ (Sheng et al., 2015), MHCII- macrophages showed a twofold reduced rate of exchange with blood-borne precursors compared with dermal MHCII+ macrophages. In parabiosis experiments involving WT and CCR2-deficient mice, the percentages of donor-derived cells found in the CCR2-deficient parabionts reached 80% and 40% of MHCII+ and MHCII- macrophages, respectively, compared with 80% for Ly-6Chigh blood monocytes (Fig. 6 B). As expected for cells linked by a precursor-product relationship, in both types of parabiosis MHCII+ and MHCII- melanophages achieved a degree of chimerism identical to that of MHCII+ and MHCII- macrophages (Fig. 6 B). Altogether, these data indicate that dermal macrophages and melanophages are related through a precursor-product relationship and that dying dermal macrophages and melanophages are continuously replenished with new ones via CCR2-dependent recruitment of circulating Ly-6Chigh blood precursors.

Comparative transcriptomic analysis of dermal macrophages and melanophages

To assess whether melanophages show a unique transcriptomic signature compared with dermal SSC-Alow macrophages that have not ingested melanin, MHCII+ and MHCII- melanophages and macrophages from the ear dermis were sorted in triplicates and subjected to gene-expression profiling. Principal component analysis (PCA) on all the genes found to be differentially expressed between at least two of the four subsets showed that the MHCII+ and MHCII- status accounted for most of the overall variability observed in the dataset (47%) and that differences between melanophages and macrophages was only the second component of variability (17%; Fig. 7 A). Insights into the biological pathways underlying these transcriptomic differences were obtained through ingenuity pathway analysis (IPA) of eight lists of genes corresponding to those differentially expressed (1) in one out of the four subsets, (2) between MHCII+ versus MHCII- cells, and (3) between melanophages and macrophages (Fig. 7 B). When compared with their MHCII- counterparts, MHCII+ macrophages and melanophages were significantly

DAPI and analyzed by microscopy for the presence of melanin. Bars: (top) 100 µm; (bottom) 20 µm. **(D)** Morphological characteristics of CD64+CCR2-SSC-Alow macrophages and CD64+SSC-Ahigh melanophages sorted from ear skin and analyzed by hematoxylin and eosin staining after cytospin onto glass slides. Two representative cells are shown for each population. Bar, 10 µm. **(E)** Morphological characteristics of CD64+SSC-Ahigh melanophages sorted from ear skin and analyzed by electron microscopy. Three representative cells are shown. Melanophages display an irregular nucleus surrounded by a prominent cytoplasm crowded with elongated melanin granules. Bars, 1 µm. Higher magnification shows pigment granules with a homogeneous and extremely dense content, attesting for its mature stage. Melanosomes are grouped together forming melanosome complexes (asterisks), but they are also singly dispersed in the cytoplasm, all of them are surrounded by a membrane. Bars, 0.5 µm. **(F)** En face section of ear dermis from *CX3CR1*Cre/+ *Rosa*lsl-tdt/+ mice analyzed by confocal microscopy for the colocalization of melanin with CD64+ CX3CR1-fate-mapped macrophages (tdtomato+). Bars: (top) 50 µm; (bottom) 10 µm. Data are representative of two to three experiments. **(G)** CD11b+CD64+CCR2- cells from the ear skin and trunk skin of B6 (telogen and anagen phases) of B6 mice were analyzed for the percentages of SSC-Alow and SSC-Ahigh cells. Data are representative of at least two experiments involving three animals per group.

A CD45$^+$Lin$^-$ live cells

B6 ear — 19.3 / 71.6
B6 albino ear — 2.72 / 86.1
BALB/c ear — 3.59 / 88.9
B6 tail skin — 8.76 / 81.1
B6 intestinal LP — 0.239 / 91.5

SSC-A / FSC-A

B

Ear Skin: B6, B6 albino, BALB/c
Tail Skin: B6

Legend:
- Dermal monocytes
- Ly-6C^{hi} MoDCs
- Ly-6C^{low} MoDCs
- MHCII$^-$ macrophages
- MHCII$^+$ macrophages
- MHCII$^-$ melanophages
- MHCII$^+$ melanophages

	Ear Skin			Tail Skin
Frequency (%)	B6	B6 albino	BALB/c	B6
Dermal monocytes	3.34 ± 1.82	6.96 ± 1.77	2.76 ± 0.65	3.90 ± 1.85
Ly-6C^{hi} MoDCs	3.51 ± 1.38	12.91 ± 3.05	3.24 ± 1.21	5.97 ± 1.78
Ly-6C^{low} MoDCs	8.42 ± 1.95	17.61 ± 4.37	13.41 ± 3.13	23.67 ± 9.34
MHCII$^-$ macrophages	22.71 ± 4.02	43.62 ± 5.10	64.79 ± 15.30	46.22 ± 7.32
MHCII$^+$ macrophages	7.02 ± 1.28	17.71 ± 4.87	15.11 ± 5.88	6.19 ± 1.63
MHCII$^-$ melanophages	46.72 ± 8.94	0.93 ± 0.21	0.52 ± 0.16	11.68 ± 2.61
MHCII$^+$ melanophages	8.29 ± 1.61	0.27 ± 0.07	0.17 ± 0.05	2.37 ± 0.71

Figure 4. **SSC-A^{high}CD64$^+$ dermal cells correspond to melanophages. (A)** CD45$^+$Lin$^-$ cells from the ear skin of B6, B6-albino, and BALB/c mice, the tail skin of B6 mice, and the lamina propria of the large intestine of B6 mice were analyzed for the percentages of SSC-A^{low} and SSC-A^{high} cells. As expected on the basis of the anatomical distribution of mouse melanocytes (Aoki et al., 2009), the lamina propria of B6 mice lacked melanophages. **(B)** Pie charts and corresponding frequencies of the indicated cells among CD11b$^+$ noncDC2 cells found in the specified anatomical location and mice strain. Data corresponding to each pie chart were averaged from six mice and the corresponding percentages (mean values ± SD) are shown below the charts. Data are representative of at least three experiments involving three to six animals per group.

enriched in annotations related to the adaptive immune response such as antigen presentation pathway, dendritic cell maturation, and cytokine signaling (IL-4, IL-6, IL-10, and IL-17). MHCII expression was also associated with a pro-inflammatory signature with higher expression of *Ccr7, Il1b, Il1r2,* and *Il6* and to immune cell chemotaxis with higher expression of *Ccl17, Ccl22, Ccl5,* and *Cxcl13* (Fig. 7 C). When compared with SSC-A^{low} macrophages, melanophages were significantly enriched in annotations related to aryl hydrocarbon receptor signaling and glutathione-mediated detoxification (Fig. 7 B) because of their expression of two genes of the glutathione S transferase family (*Gstm1* and *3*; Table S1). High and selective expression by melanophages of genes coding for a lysosomal ATPase and a cystein protease (*Atp6v0d2* and *Ctsk,* respectively) led to their enrichment for the annotation phagosome maturation (Fig. 7 B and Table S1), a feature consistent with the fact that they are laden with melanosomes.

Melanophages are found in melanocytic melanoma

Tumors depend on the supportive functions of macrophages. Clusters of melanophages have been observed in the periphery

of the nevi found in the dermis of mice expressing oncogenic mutated form (BrafV600E) of the serine-threonine-specific protein kinase BRAF (Dhomen et al., 2009). To determine whether such melanoma-associated melanophages correspond to CD64$^+$SSC-A^{high} cells, B6-albino mice, which lack melanophages, were injected with melanocytic (B16) or amelanoctyic (Braf^{V600E}) melanoma cells. Analysis of CD45$^+$Lin$^-$Siglec-F$^-$ cells isolated from tumor masses 14 to 18 d after inoculation showed that SSC-A^{high} cells were present only in the melanocytic melanoma (Fig. 8 A). Their morphology was similar to that of the melanophages identified in the B6 dermis (Fig. 8 B) and they had a CD11b$^+$CD64$^+$F4/80$^+$ phenotype (Fig. 8 C).

The melanophages that are identifiable in melanocytic melanoma constitute a unique thread permitting revisiting the phenotype of tumoral macrophages. For instance, the presence of CD64 and absence of Ly-6C permit readily distinguishing macrophages in steady-state tissues (Tamoutounour et al., 2013), and it has been assumed that such a feature holds true within the tumor microenvironment (Salmon et al., 2016). Our analysis of the melanophages found in melanocytic tumors showed, however,

A

B
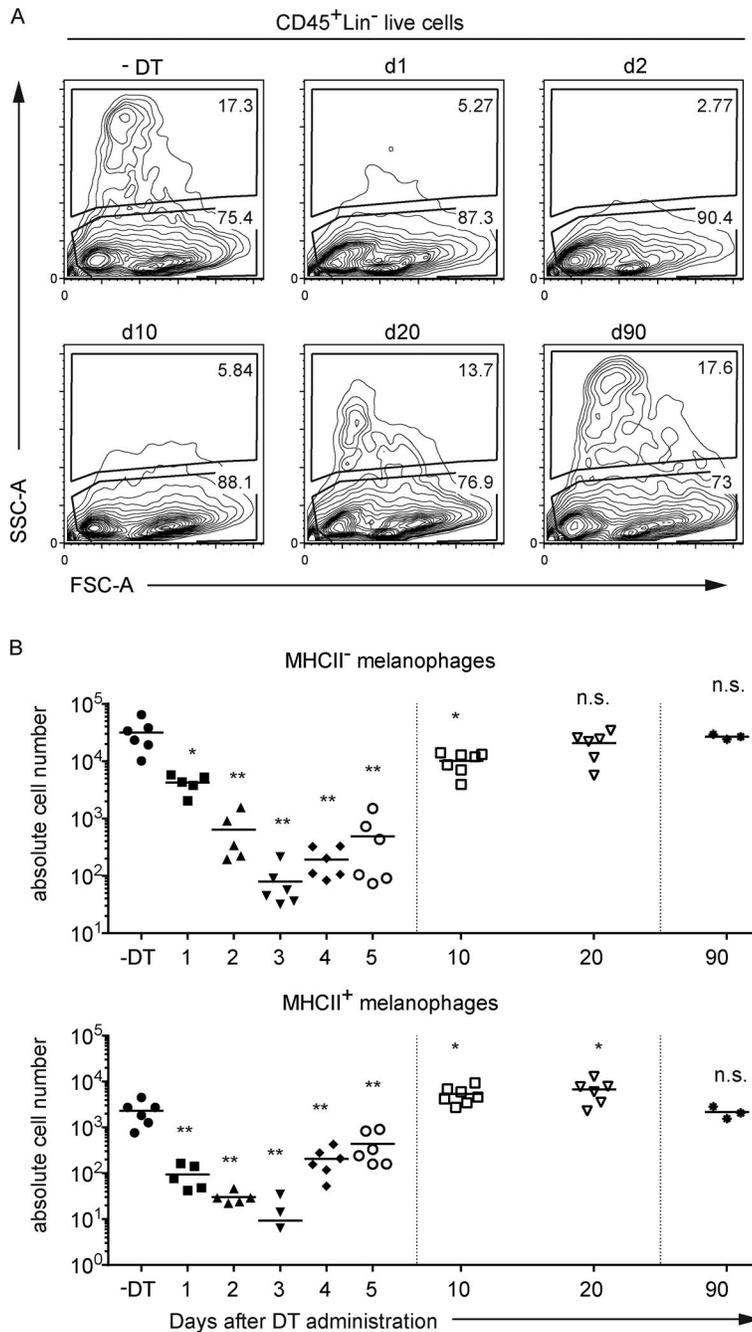
Figure 5. **SSC-A^{high}CD64$^+$ melanophages showed a protracted kinetics of replenishment after DT treatment compared with SSC-A^{low} macrophages. (A)** CD45$^+$Lin$^-$ cells from the ear skin of CD64^{dtr} mice were analyzed for the percentages of SSC-A^{low} and SSC-A^{high} cells before (-DT) or at the specified time points after DT treatment. **(B)** Quantification of the results in A are shown for the MHCII$^+$ and MHCII$^-$ cells found among the SSC-A^{high} melanophages. Each symbol corresponds to a mouse and the mean (horizontal bar) is indicated. Data are representative of two to three independent experiments involving three to six animals per group. n.s., P > 0.05; *, P ≤ 0.05; **, P ≤ 0.01; unpaired Student's t test.

that most of them expressed Ly-6C (Fig. 8 C). Therefore, analysis of the melanophages found in melanoma constitute a unique decision support tool permitting to determine whether markers defined as macrophage-specific under steady-state conditions keep or lose their discriminatory potential within the tumor microenvironment.

Skin macrophages capture and retain tattoo pigment particles
Using the CD64^{dtr} mouse model and benefiting of our knowledge on melanophages, we determined next the identity, origin, and dynamics of the skin myeloid cells that are capable of capturing and retaining tattoo pigment particles. The frequency of melanophages in the tail skin of B6 mice is fourfold lower than that of melanophages in ear dermis and reflects its scarcity in

melanocytes. Moreover, because of their reduced melanin content tail skin melanophages barely merged in the SSC-A^{high} gate, the lower limit of which that was defined by using B6 albino ear (Fig. 4, A and B). Accordingly, we used tail skin of B6 mice to monitor the appearance in the almost-empty SSC-A^{high} gate of those cells that have captured the bright green pigment particles that are contained in the tattooing ink paste used in the present study. Analysis of the percentages of SSC-A^{low} and SSC-A^{high} cells found among the CD45$^+$Lin$^-$ cells isolated from the skin of tails that were tattooed 3 wk before analysis showed that they contained a unique population of SSC-A^{high} cells compared with untreated mice (Fig. 9 A). Further characterization of those SSC-A^{high} cells showed that they had a CD24^{low}CD11b$^+$CD64$^+$CCR2$^{- to low}$ phenotype (Fig. 9 A), which was identical to that observed for SSC-A^{high}
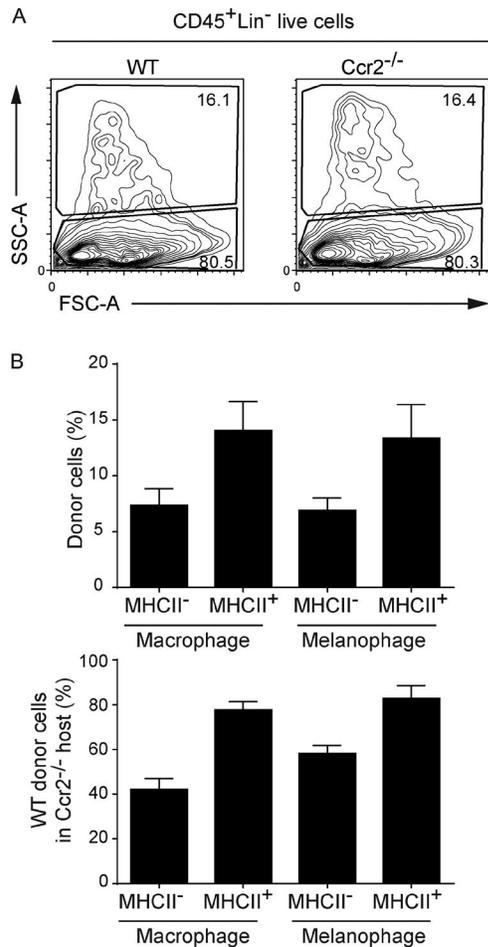
Figure 6. **Prenatal and adult origins of SSC-A^{high}CD64$^+$ melanophages.**
(A) CD45$^+$Lin$^-$ cells from the ear skin of B6 (WT) and *Ccr2$^{-/-}$* mice were analyzed for the percentages of SSC-A^{low} and SSC-A^{high} cells. **(B)** Percentages (mean values ± SD) of donor chimerism in MHCII$^+$ and MHCII$^-$ dermal macrophages and MHCII$^+$ and MHCII$^-$ melanophages found in the skin dermis of parabiotic mice involving either CD45.1 and CD45.2 WT parabionts or CD45.1 WT and CD45.2 *Ccr2$^{-/-}$* parabionts. No macrophages or melanophages originating from CCR2-deficient mice were found in the dermis of WT partners. Data are representative of two to three independent experiments involving two to four animals per group.

melanophages and SSC-A^{low} macrophages (Fig. 3 B). Cytospin analysis of SSC-A^{high} cells sorted from tattooed tail skin showed that they were large cells containing prominent cytoplasmic vacuoles loaded with green material, whereas SSC-A^{low} dermal macrophages and cDCs contained no green tattoo pigment (Fig. 9 B). None of the CD45$^-$ skin cells, which mostly comprise keratinocytes, contained green material (not depicted). Therefore, 3 wk after tail tattooing, the green pigment particles present at the site of tattooing were primarily found within dermal macrophages.

Cycles of pigment capture–release–recapture account for long-term tattoo persistence

We used CD64^{dtr} mice to ablate dermal CD64$^+$ macrophages laden with green pigment particles ("green" macrophages in short) and to determine whether their death results in tattoo vanishing. Accordingly, CD64^{dtr} mice that had the skin of their tail tattooed with green tattoo ink paste 3 wk before were treated with

DT twice and 24 h apart. Analysis of tattooed skin of those mice for the presence of SSC-A^{high} green macrophages showed that they were as expected all ablated within 2 d after DT treatment and that, akin to melanophages, their pool was slowly reconstituted after DT injection (Fig. 9 C). Their granularity, reflecting green-particle content per cell, increased with time and 90 d after DT injection reached levels identical to those present just before DT treatment (Fig. 9, A and C). The pool of SSC-A^{high} cells that was replenished 90 d after DT treatment was exclusively composed of green macrophages with a morphology and CD24^{low}CD11b$^+$ CD64$^+$CCR2$^{- to low}$ phenotype resembling those of green macrophages observed pre-DT treatment (Fig. 9 D and not depicted).

Considering that no green tattoo ink paste was reapplied after DT treatment, it is likely that most of the green pigment particles released after DT-induced green macrophage death remained in an extracellular form at the site of tattooing where they were progressively recaptured by incoming dermal macrophages originating from circulating Ly-6C^{high} blood monocytes (see model A in Fig. 10). Consistent with that model, cytospin preparation of the total cell suspension from tail skin showed that before DT treatment green pigment particles were all associated with cells that had typical features of tissue macrophages, whereas 2 d after the last DT injection no green macrophages were left (Fig. 9 C) and the green pigment particles that were spun down with the cells were all extracellular (Fig. 9 E). Importantly, macroscopic examination of tattooed tails showed that even at time points when green macrophages were absent and green pigment particles were extracellular (for instance, day 2 after DT), the tattoo kept the appearance it had just before DT treatment (Fig. 9 F). Therefore, despite the fact that the green tattoo pigments went, over 90 d, through a full cycle of capture–release–recapture, the tattoo kept its macroscopic appearance.

To further support our pigment capture–release–recapture model without relying on DT ablation, CD45.1$^+$ B6 mice were tattooed on the tail. The tattooed tail skin was explanted and grafted on the skin of the back of CD45.2$^+$ B6 albino mice. Analysis of the myeloid cells present in the graft 6 wk after transplantation showed that most of the SSC-A^{high} cells found among CD11b$^+$ CD64$^+$CCR2$^-$ cells were of host origin, suggesting that green tattoo pigments were released from the CD45.1$^+$CD11b$^+$CD64$^+$CCR2$^-$ SSC-A^{high} cells originally present in the donor graft and captured by incoming CD45.2$^+$CD11b$^+$CD64$^+$CCR2$^-$ macrophages of host origin (Fig. 9 G). As discussed below, those findings provide a cellular basis for long-term tattoo persistence and have implications for improving strategies aimed at removing tattoos.

Discussion

We used a novel model of DT-induced depletion of macrophages to generate niche availability without triggering inflammation and showed that the pool of adult dermal macrophages can be fully reconstituted from circulating Ly-6C^{high} monocytes. By using a model of DT-mediated depletion of liver Kupffer cells, circulating Ly-6C^{high} monocytes were also found capable of colonizing the emptied liver niches and of adopting a Kupffer cell identity (Scott et al., 2016). Likewise, transferred BM-derived monocytes were able to colonize the empty alveolar macrophage
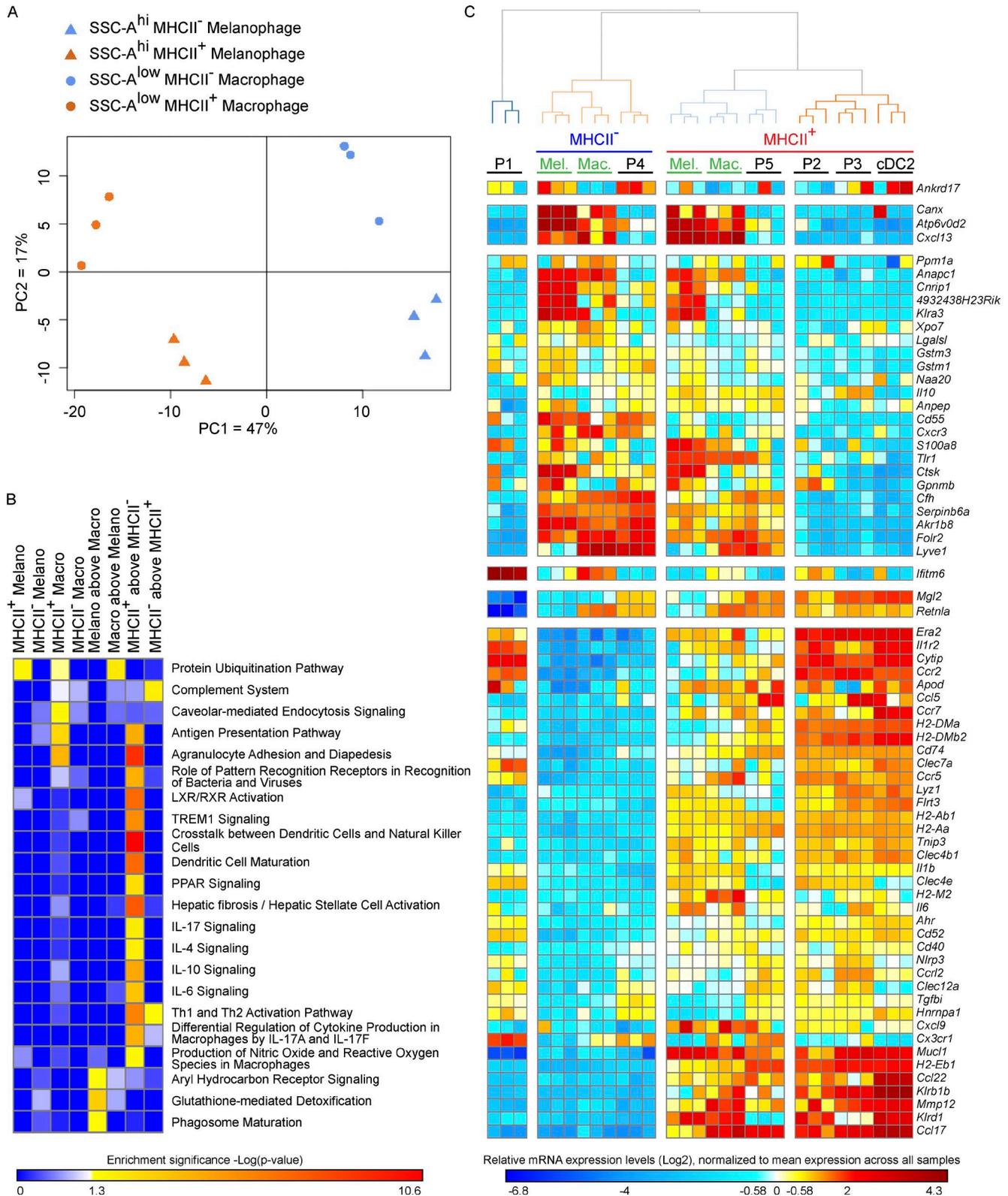
Figure 7. Gene expression profiling of MHCII+ and MHCII− melanophages and macrophages from steady-state dermis. MHCII+ and MHCII− CD64+CCR2−
SSC-A^low macrophages and MHCII+ and MHCII− CD64+SSC-A^high melanophages were sorted in triplicates from ear skin and subjected to gene-expression
profiling (Affymetrix 1.0ST). **(A)** PCA of gene expression by MHCII+ and MHCII− dermal macrophages and MHCII+ and MHCII− melanophages, based on all the
1,054 unique genes differentially expressed between at least one pair of experimental conditions. The percentage of overall variability of the dataset is indicated
along each PC axis. **(B)** Heat map representation of selected functions and pathways found enriched by IPA for the lists of genes differentially expressed in one
of the three cell types, between MHCII+ versus MHCII− cells, or between melanophages and macrophages. **(C)** Heat map showing the expression pattern across

niche of neonatal CSF2RB-deficient mice and generate alveolar macrophages (van de Laar et al., 2016). Therefore, our data showed that the capacity for Ly-6C^{high} blood monocytes to replenish macrophages after DT-induced ablation also extends to the skin dermis. Moreover, we characterized the melanophages that are present in large numbers in the normal ear dermis of mice with a black coat, demonstrating that they correspond to dermal macrophages that have ingested melanosomes originating from neighboring melanocytes.

Limited information has been provided on the identity of the cells that are found in tattooed skin biopsies and capable of retaining tattoo pigment particles. By capitalizing on the knowledge gained on melanophages and on the functionalities offered by CD64^{dtr} mice, we conducted the first systematic analysis of the identity, origin, and dynamics of the skin myeloid cells that are capable of capturing and retaining tattoo pigment particles. The tattooing process consists of inserting water-insoluble pigment of the desired color into the dermis layer of the skin. Tattoo pigments are primarily metal salts in the submicrometer range. Immediately after tattooing, a fraction of pigments is shed with the epidermis or transported away from the dermis via lymphatic vessels. We demonstrated that the pigment particles that remain at the site of injection and cause the long-term tattoo color were exclusively found within dermal macrophages. Zaba et al. (2007) previously identified a population of cells located in the human dermis that was positive for factor XIIIA and the macrophage scavenger receptor CD163 that lacked CD11c and BDCA-1 and weakly activated allogenic T cells. Those cells have structural and ultrastructural features of macrophages and in biopsies of tattoos they were selectively laden with granular pigments. The fate of tattoo pigment injected into dermal tissues has been studied in the past, and fibroblasts were considered the primary long-term reservoir of the pigment granules (Ferguson et al., 1997; Elsaie et al., 2009). However, the morphological study of Zaba et al. (2007) and our present data combining multiparameter cytometry and the use of CD64^{dtr} "depleter" mice demonstrate that dermal macrophages constitute the primary store of dermal tattoo pigment in both mice and humans.

Although the dermis lacked macrophages for approximately 1 wk after DT treatment and it took several more weeks for the incoming macrophages to scavenge the released cell-free tattoo pigments, no macroscopic modification of the tattoo occurred. Before our study, the longevity of the undefined tattoo-pigment-laden cells found in the dermis was thought to be in the same order of that of a human adult, thereby accounting for long-term tattoo persistence (Fig. 10 B). Based on the present results, an alternative model for long-term tattoo persistence can be proposed. It takes into consideration the facts that the macrophages found in the dermis of adult mice are continuously replenished from circulating monocytes to compensate
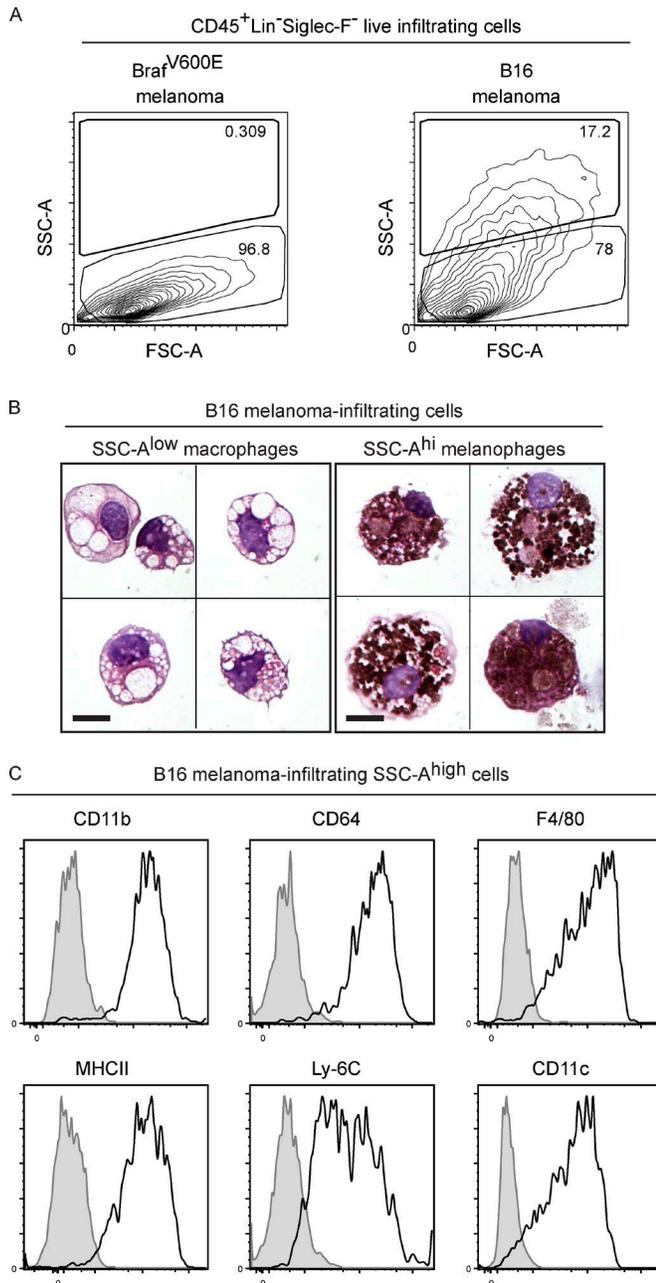
for the loss of dying macrophages and that most of the tattoo particles that are released from macrophages after DT treatment of CD64^{dtr} mice remain in situ and are recaptured by incoming macrophages. According to the pigment capture–release–recapture model (Fig. 10 A), in physiological conditions, when tattoo-pigment-laden macrophages die during the course of adult life, neighboring macrophages recapture the released pigments and ensure in a dynamic manner the macroscopic stability and long-term persistence of tattoos. Note that, in contrast to dermal cDCs, dermal macrophages do not have the capacity to migrate to draining LNs under normal and inflammatory conditions (Tamoutounour et al., 2013), an essential property for insuring tattoo persistence. Whether the pigment capture–release–recapture model of tattoo persistence applies to humans remains to be determined. In the case of the melanophages found in the human dermis, it has been suggested that they persist for years through longevity rather than continual renewal (Bigley et al., 2011).

Professional tattoos last for years or decades, and when no longer desired, they can be removed through the use of quality-switched lasers. Laser pulses lead to lysis of the tattoo-pigment-laden cells, fragmentation of the tattoo pigments, and their lymphatic transportation. Several cycles of laser treatment are required to achieve tattoo removal, and some tattoos remain immune to full removal. These difficulties are generally accounted for by the fact that a fraction of the fragmented pigment particles remains at the tattooing site and are recaptured by neighboring cells, a possibility formally demonstrated here by using the CD64^{dtr} model. Considering the long duration needed for the reconstitution of the pool of dermal macrophages and the recapture of the whole released pigments, tattoo removal can be likely improved by combining laser surgery with the transient ablation of the macrophages present in the tattoo area. As a result, the fragmented pigment particles generated by using laser pulses will not have the possibility to be immediately recaptured, a condition increasing the probability of having them drained away via the lymphatic vessels.

In conclusion, we have validated a new model of DT-mediated depletion of tissue-resident macrophages, monocytes, and monocyte-derived cells in which DCs are spared. By permitting the emptying of the niche occupied in the skin dermis and intestinal lamina propria by CD64$^+$ myeloid cells, the CD64^{dtr} mouse model showed that all the mo-DC and macrophage subsets that were present in adult skin and intestine before DT treatment can be readily reconstituted from circulating Ly-6C^{high} monocytes. Furthermore, we showed that the myeloid cells of the ear skin dermis are dominated by melanophages, and we determined their origin and dynamics. Benefiting by our knowledge on melanophages, we determined the identity, origin, and dynamics of the skin myeloid cells that are capable of capturing tattoo-pigment particles and showed that

skin monocytes (P1), mo-DCs (P2, P3), macrophages (P4, P5, Mac), melanophages (Mel), and cDC2s of selected genes contributing to IPA enrichments for the SSC-A^{low} macrophage, SSC-A^{hi} melanophage, and MHCII$^-$ versus MHCII$^+$ transcriptomic signatures. The cell samples which names are in black font on the top of the heat map originate from Tamoutounour et al. (2013), where the P4 and P5 cells correspond to the MHCII$^-$ and MHCII$^+$ macrophages from the present study. The exhaustive lists of genes responsible for the IPA enrichments shown in B are provided in Table S1.

A

CD45⁺Lin⁻Siglec-F⁻ live infiltrating cells

B

B16 melanoma-infiltrating cells

C

B16 melanoma-infiltrating SSC-A^{high} cells

Figure 8. **SSC-A^{high}CD64$^+$ melanophages can be found in melanocytic melanoma. (A)** B6-albino mice were injected subcutaneously with 10^5 amelanocytic (Braf^{V600E}) or melanocytic (B16) melanoma cells. CD45$^+$Lin$^-$Siglec-F$^-$ cells were isolated from tumor masses 14–18 d after inoculation and analyzed for the percentages of SSC-A^{low} and SSC-A^{high} cells. Note that Siglec-F staining permits elimination of eosinophils. **(B)** Morphological characteristics of representative SSC-A^{high} melanophages and SSC-A^{low} macrophages sorted from B16 melanoma tumor masses after cytospin onto glass slides. Four representative cells are shown for each population. Panels are made of two to four concatenated images. Bars, 10 µm. **(C)** Analysis of CD45$^+$Lin$^-$Siglec-F$^-$ SSC-A^{high} cells isolated from B16 melanoma tumor masses 14 d after inoculation for CD11b, CD64, F4/80, MHCII, Ly6C, and CD11c expression. Appropriate isotype controls are shown for each of the analyzed markers. Data are representative of at least three experiments involving three animals per group.

they correspond exclusively to dermal macrophages. Based on those results, we proposed a dynamic model that accounts for long-term tattoo persistence and suggest that tattoo removal

can be improved by combining laser surgery with the transient and specific ablation of the macrophages present in the tattooed area. Finally, we showed that melanocytic melanoma host readily identifiable melanophages that permit determining whether markers defined as macrophage-specific under steady-state conditions keep or lose their discriminatory potential within the tumor microenvironment.

Materials and methods

Mice

Ccr2$^{-/-}$ mice have been described (Jung et al., 2000). *Cx3cr1*$^{cre/+}$ (MW126Gsat) mice were generated by N. Heintz (The Rockefeller University, GENSAT, New York) and purchased from MMRRC. *Rosa*$^{lsl-tdt/+}$ (Ai14[RCL-tdT]-D) have been described (Madisen et al., 2010) and purchased from The Jackson Laboratory. Generation of *Fcgr1-IRES-EGFP-hDTR* gene-targeted mice is described below. C57BL/6 (B6) and BALB/c mice were purchased from Janvier and B6 albino (B6[Cg]-Tyr$^{c-2J/J}$) and CD45.1 C57BL/6 mice from Charles River. All mice, except BALB/c, were maintained on a B6 background. Mice were housed under specific pathogen–free conditions, and in vivo procedures were performed following protocols approved by the Ethics Committee of Marseille in accordance with institutional, national, and European directives for animal care (approvals APAFIS 779–2015 0605 10534083 and APAFIS 781–2015 0605 14006182).

Construction *Fcgr1-IRES-EGFP-hDTR* mice

A 6.2-kb genomic fragment encompassing exons 4 to 6 of the *Fcgr1* gene (ENSMUSG00000015947) was isolated from a BAC clone of B6 origin (clone RP23-427P23; http://www.lifesciences.sourcebioscience.com). By using ET recombination, an IRES-EGFP-2A-hDTR-loxP-Cre-neoR-loxP cassette was introduced in the 3′ untranslated region of the *Fcgr1* gene, 33 bp downstream of the stop codon. The targeting construct was abutted to a cassette coding for the DT fragment A expression cassette and linearized with Pme1. JM8.F6 C57BL/6N embryonic stem (ES) cells (Pettitt et al., 2009) were electroporated with the targeting vector. After selection in G418, ES cell clones were screened for proper homologous recombination by Southern blot. When tested on Sca1-digested genomic DNA, the 3′ single-copy probe used to identify proper recombination events hybridized to a 7.0-kb WT fragment and to a 10.3-kb recombinant fragment. When tested on HindIII-digested genomic DNA, the 5′ single-copy probe used to identify proper recombination events hybridized to a 10.7-kb WT fragment and to a 6.3-kb recombinant fragment. A neomycin-specific probe was used to ensure that adventitious nonhomologous recombination events had not occurred in the selected ES clones. Properly recombined ES cells were injected into FVB blastocysts. Germline transmission led to the self-excision of the loxP-Cre-NeoR-loxP cassette in male germinal cells. *Fcgr1-IRES-EGFP-hDTR* mice were identified by PCR of tail DNA. The pair of primers, sense 5′-CCCTTCCTCCCAGTGACAGTACTG-3′ and antisense 5′-TGAACCCATCCACCCTGTGAG-3′, amplifies a 402-bp band in case of the WT *Fcgr1* allele, whereas the pairs of primers, sense 5′-CCCTTCCTCCCAGTGACAGTACTG-3′ and antisense 5′-CCTGCAAAGGGTCGCTACAGA-3′, amplified a 349-bp
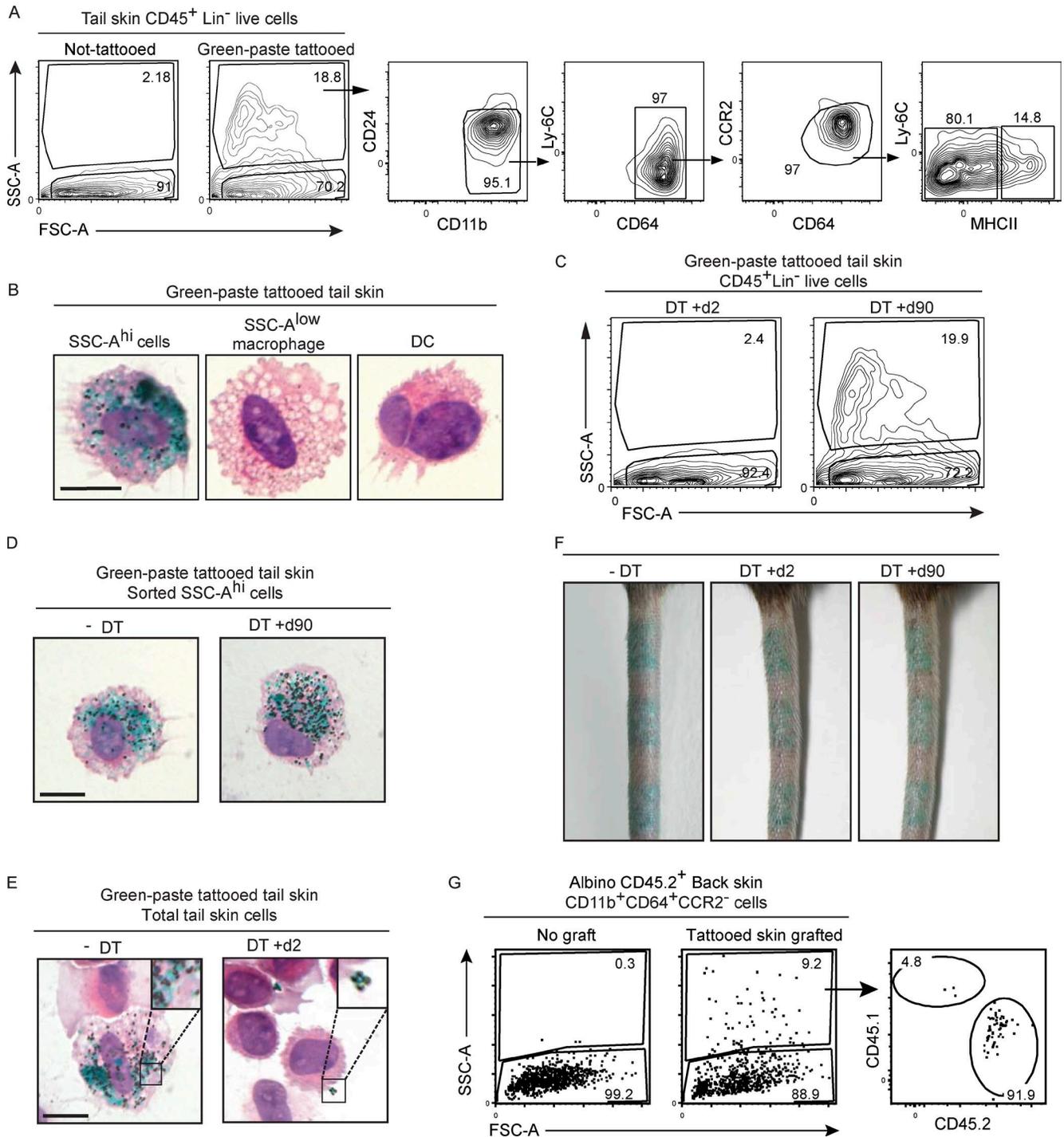
Figure 9. **Dermal macrophages are responsible for uptake and storage of tattoo pigment particles. (A)** CD45⁺Lin⁻ cells from the tail skin of B6 mice that were left untreated or tattooed with green tattoo ink paste 3 wk before isolation were analyzed for the percentages of SSC-A^low and SSC-A^high cells. SSC-A^high cells were further analyzed by using a gating strategy resolving cDC2s, monocytes, mo-DCs, and macrophages (Fig. S1 A). **(B)** Morphological characteristics of representative SSC-A^high cells (green macrophages), SSC-A^low cells (macrophages), and cDC2s sorted from tail skin of B6 mice tattooed with green tattoo paste 3 wk before isolation and analyzed by hematoxylin and eosin staining after cytospin onto glass slides. Bar, 10 µm. **(C)** Tails of CD64^dtr mice were tattooed with green tattoo paste. 3 wk after, mice were treated twice and 24 h apart with 1 µg DT, and tail skin was analyzed 2 or 90 d after the last DT injection for the percentages of SSC-A^low and SSC-A^high cells found among CD45⁺Lin⁻ cells. **(D)** SSC-A^high cells were sorted from the tail skin of CD64^dtr mice that were tattooed with green tattoo paste and either left untreated (-DT) or treated with DT and analyzed 90 d (DT + d90) after DT treatment. Sorted cells were analyzed by hematoxylin and eosin staining after cytospin onto glass slides. One representative cell is shown for each population. Bar, 10 µm. **(E)** Tail skin of CD64^dtr mice that were tattooed with green tattoo paste and either left untreated (-DT) or treated with DT and analyzed 2 d (DT + d2) after DT treatment was digested, and the resulting cell suspension was directly analyzed by hematoxylin and eosin staining after cytospin onto glass slides. Insets show magnification of selected areas. Bar, 10 µm. **(F)** Macroscopic view of the tails of CD64^dtr mice that were tattooed with green tattoo ink paste and either left untreated (-DT) or treated

band in the case of the *Fcgr1-IRES-EGFP-hDTR* allele. Because of its low level of expression, the EGFP reporter was not used in the present study.

Isolation of monocytes, macrophages, and DCs from tissues and tumors

To isolate myeloid cells from ear skin, ears were processed as described (Bouladoux et al., 2017). In brief, ears were split into ventral and dorsal parts and incubated for 105 min at 37°C in RPMI containing 0.25 mg/ml Liberase TL (Roche Diagnostic Corp.) and 0.5 mg/ml DNase I (Sigma Aldrich). Digested tissue was homogenized by using Medicons and Medimachine (Becton Dickinson) to obtain homogenous cell suspensions. To isolate myeloid cells from tail skin, the skin was separated from the muscle and the vertebra and cut into small pieces and then digested in RPMI with Liberase TL and DNase as described for ear skin. The digested tissue was homogenized by using C Tubes and GentleMACS Dissociator (Miltenyi Biotec). To isolate myeloid cells from the lamina propria of the large intestine, the large intestine was opened longitudinally, cut into pieces, and washed in HBSS. The epithelial layer was eliminated by two incubations of 20 and 30 min in HBSS containing 2 mM EDTA. Intestinal pieces were washed twice in HBSS and then digested in RPMI medium containing 10% FCS, 1 mg/ml Collagenase 8 (Sigma Aldrich), and 30 ng/ml DNase I. Tissue was homogenized in C Tubes and GentleMACS Dissociator. Light-density cells were then purified by centrifugation on a 70–40% Percoll gradient (GE Healthcare). To isolate myeloid cells from tumor mass, tumors were cut into small pieces and then digested in RPMI medium containing 5% FCS, 0.8 mg/ml Collagenase 4 (Worthington), and 0.2 mg/ml DNase I for 40 min at 37°C. The digested tissue was homogenized by using C Tubes and GentleMACS Dissociator (Miltenyi Biotec).

Analysis of blood cells

Blood was collected in EDTA-containing tubes and then transferred to Trucount Absolute Counting Tubes (Becton Dickinson). Red blood cells were lysed with BD FACS Lysing Solution (Becton Dickinson). The absolute number of cells present in a given volume was determined by using the bead-to-cell ratio.

Antibodies

APC-Vio770–conjugated anti-NK1.1 (PK136), anti-CD3 (17A2), anti–Ly-6G (1A8), and anti-CD19 (6D5) were from Miltenyi Biotec. Biotin-conjugated anti–mouse-MERTK (BAF591) and PE-conjugated anti-CCR2 (475301) were from R&D. BV711-conjugated anti-CD11b (M1/70); BV605-conjugated anti-CD11c (N418); FITC-conjugated anti-CD43 (S7); Alexa Fluor 700–conjugated anti-CD45.1 (A20); Alexa Fluor 700–conjugated rat IgG2b κ isotype control (R35-38);

FITC-conjugated anti-CD45.2 (104); APC-conjugated anti-CD64 (X54-5/7.1); FITC-, PE-CF594-, and BV421-conjugated anti–Ly-6C (AL-21); BV650-conjugated anti-NK1.1 (PK136); BV421-conjugated anti–Siglec-F (E50-2440); biotin-conjugated anti–Ly-6C (AL-21); and biotin-conjugated anti-CD103 (M290) were from BD PharMingen. PE-Cy5–conjugated anti-CD24 (M1/69), BV650-conjugated anti-CD45.1 (A20), PE-conjugated anti–Ly-6G (1A8), Pe-Dazzle–conjugated anti-CD45.2 (104), APC-conjugated anti-F4/80 (BM8), APC-conjugated rat IgG2a κ isotype control (RTK2758), APC-conjugated anti-CD11c (N418), APC-conjugated Armenian hamster IgG isotype control (HTK888), APC-conjugated anti-CD5 (53-7.3), APC-conjugated anti-CD19 (6D5), APC-Cy7–conjugated anti-CD11b (M1/70), FITC-conjugated anti-CD11b (M1/70), FITC-conjugated rat IgG2b κ isotype control (MRG25-8T), BV711-conjugated anti-CD64 (X54-5/7,1), BV711-conjugated mouse IgG1 κ isotype control (MOPC-21), and BV510- and Alexa-700–conjugated anti–MHC Class II (IA/I-E; M5/114.15.2) were from Biolegend. PE-Cy5.5–conjugated anti-CD45 (30-F11) and Pe-Cy7–conjugated anti-CD115 (AFS98) were from eBioscience. Biotin-conjugated antibodies were detected by using streptavidin conjugated with PE-CF594 or Pe-Cy7 (BD PharMingen).

Flow cytometry

Cells were stained and acquired on a FACS LSRII system and analyzed with FlowJo software (Tree Star). Neutrophils and B, T, and NK cells were systematically gated out by using a Lin$^+$ gate (Fig. S1 and Fig. 2).

Cell sorting

The different cell types were sorted on a FACS Aria II according to the marker combination specified on Fig. S1 A and Fig. 3. For microarrays (Affymetrix 1.0ST), cells were sorted directly in lysis buffer provided from the Qiagen RNAeasy PLUS extraction kit.

Cell morphology

Sorted cells were spun onto Shandon Cytoslides with a Thermo Shandon Cytospin 4 cytofuge (4 min at 400 g), fixed with methanol and stained with hematoxylin and eosin.

Electron microscopy

Sorted cells were incubated at 37°C on poly-Lysine–coated cover slides. After 30 min, attached cells were fixed by using 2% glutaraldehyde in 0.1 M cacoldylate buffer, pH 7.4 for 1 h, postfixed for 1 h with 2% buffered osmium tetroxide, dehydrated in a graded series of ethanol solution, and then embedded in epoxy resin. Images were acquired with a digital camera Quemesa (SIS) mounted on a Tecnai Spirit transmission electron microscope (FEI Company) operated at 80 kV.

---

with DT and analyzed 2 (DT + d2) and 90 d (DT + d90) after DT treatment. Data are representative of at least three experiments. **(G)** CD11b$^+$CD64$^+$CCR2$^-$ cells from the back of untreated CD45.2 albino mice or from the back of CD45.2 albino mice previously grafted with green-tattooed tail skin from CD45.1 B6 animals were analyzed for the percentages of SSC-A^{low} and SSC-A^{high} cells. The SSC-A^{high} CD64$^+$ cells found in the back of the grafted CD45.2 albino mice were further analyzed for the percentages of CD45.1 (donor) and CD45.2 (host) expression. Data are representative of two to three independent experiments involving two to four animals per group.
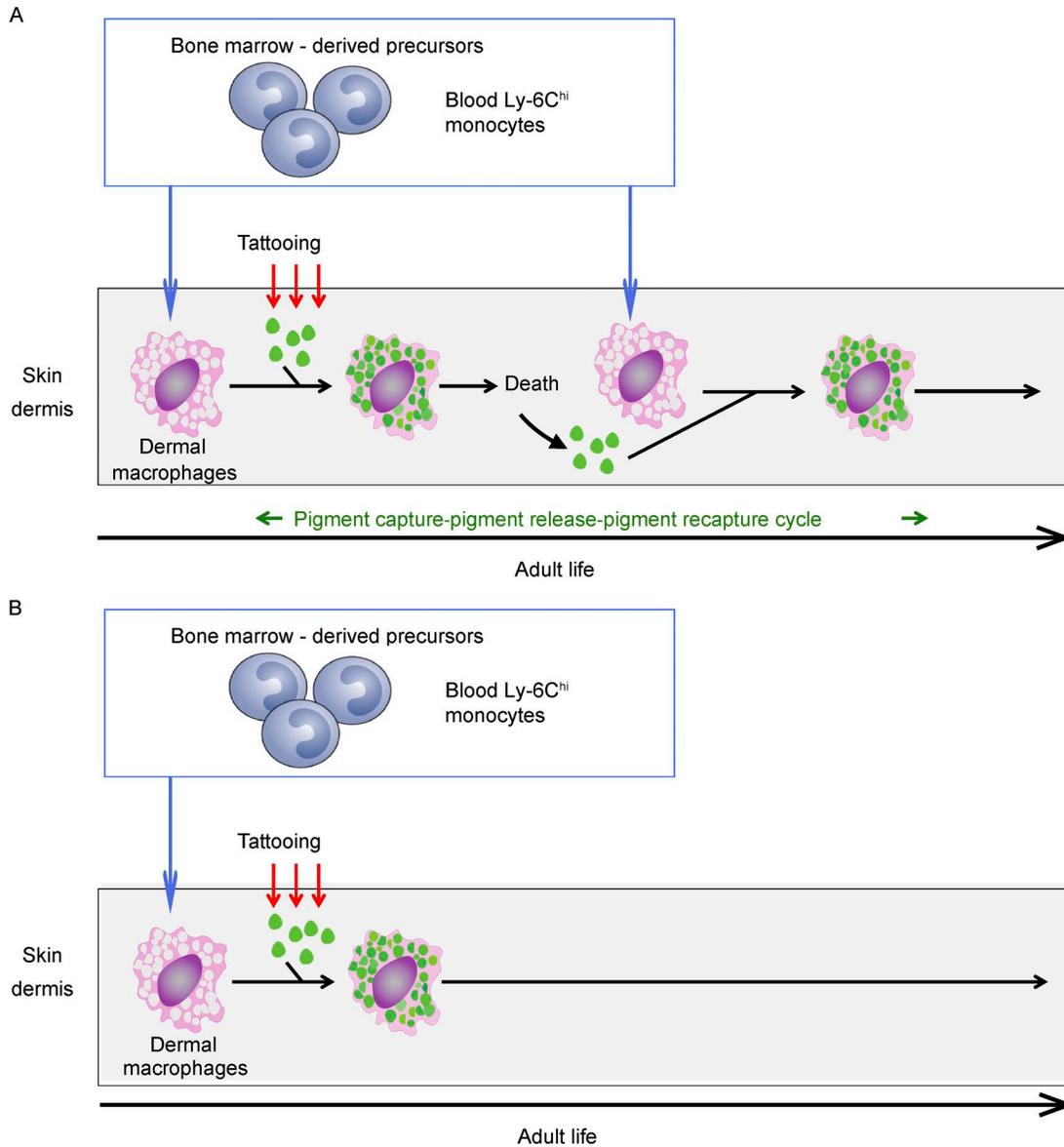

Figure 10. **Models accounting for tattoo persistence. (A)** The pigment capture–release–recapture model. Analysis of parabiotic mice that share a blood supply showed that the macrophage pool found in the noninflammatory dermis of adult mice is continuously replenished from circulating monocytes, thereby permitting replacement of dying macrophages. Upon tattooing, pigment particles (green) are captured by dermal macrophages. With time, macrophages laden with tattoo pigment particles die and release the tattoo pigment particles. Because of their size, those particles remain in an extracellular form at the site of tattooing where they are recaptured by neighboring or incoming macrophages. During the adult life, several cycles of pigment capture–release–recapture can occur, accounting for long-term tattoo persistence. **(B)** The "longevity" model. Although data on dermal macrophage dynamics (Tamoutounour et al., 2013; McGovern et al., 2014; and this paper) speak in favor of a pigment capture–release–recapture model, the possibility that a few dermal macrophages including those laden with green tattoo pigments had a longevity of the same order of adult mice cannot be excluded.

Confocal microscopy

Trunk and ear skin pieces were fixed in Antigen Fix (Microm Microtech) for 2 h, washed in 0.1 M phosphate buffer, and dehydrated overnight in 30% sucrose in 0.1M phosphate buffer. Tissues were snap frozen, and 25-µm sections were stained with DAPI. To obtain an en face section of ear dermis, the dorsal part was split from the ventral one 2 h after intradermal ear injection of CD64-APC (2 µg), fixed in Antigen Fix for 2 h, washed in phosphate buffer, stained with DAPI, and clarified with Rapiclear 1.47 (SunJin Lab). Immunofluorescence confocal microscopy was performed by using a Zeiss LSM 880 confocal microscope. Separate images were collected for each fluorochrome and merged to obtain a multicolor image. Final image processing was performed with Imaris software (Bitplane) and Adobe Photoshop.

RNA isolation and microarray analysis

Transcriptomic and bioinformatics analyses were performed as previously described (Tamoutounour et al., 2013). To perform a PCA focused on all variability across the four biological samples examined (Fig. 7 A), we selected all ProbeSets showing a fold change ≥1.2 between at least one pair of conditions, taking into account only those ProbeSets nonambiguously annotated

to one gene only and further keeping only the highest ProbeSet for each gene. This led to selection of 1,054 unique genes. To select the genes showing a significant differential expression in one type of condition compared with the other three, between MHCII[+] versus MHCII^{−} cells, or between melanophages and macrophages (Fig. 7 B), we used the GeneSign module of the Bubble-GUM software using the metrics Minimal pairwise (Mean[test]/Mean[ref]) with a linear fold change threshold of 1.5 and a P value threshold of 0.05. The microarray data have been deposited in the GEO database under accession number GSE103339.

Generation of parabiotic mice

Parabiotic mice were generated by using 8–9-wk-old male mice as described previously (Tamoutounour et al., 2013). For WT-WT parabiosis, CD45.1 B6 mice were sutured together with CD45.2 B6 mice, whereas for WT-*Ccr2*^{−/−} parabiosis, WT CD45.1 B6 mice were sutured with *Ccr2*^{−/−} CD45.2 B6 mice and subsequently treated with Bactrim for 8 wk before analysis.

In vivo depletion of CD64^{+} cells

CD64[dtr] mice were injected intraperitoneally twice and 24 h apart with 1 µg DT (Calbiochem, EMD Millipore) in PBS. *CD64*[dtr] mice injected with PBS showed no ablation of monocyte-derived cells and macrophages.

Tumor model

B6-albino mice were injected subcutaneously with 10[5] amelanocytic (Braf[V600E]) or melanocytic (B16) melanoma cells (Brown et al., 2001; Zelenay et al., 2015).

Tattooing

Tattooing was performed on the tail skin of mice under general anesthesia. Tail skin was tattooed by using the Animal Tattoo Ink Paste (Ketchum Mfg. Co, Inc.) and a 25-gauge needle. The ink-coated needle permits ink delivery in a topical manner. Before analysis, mice were kept for at least 3 wk until complete healing of the treated skin.

Skin grafting

CD45.1 B6 mice were tattooed as described above. After 5 wk, the tattooed tail skin was explanted and grafted on the back of CD45.2 albino mice under general anesthesia. The back skin of the host was analyzed 6 wk after the graft.

Statistical analyses

The unpaired Student *t* test was used for statistical analyses with GraphPad Prism software.

Online supplemental material

Fig. S1 shows the gating strategy used to identify CD11b^{+} cell subsets within the skin of WT and CD64[dtr] mice. Fig. S2 shows the ablation of CD64^{+} cells present in the lamina propria of the large intestine upon DT treatment of CD64[dtr] mice. Fig. S3 shows the replenishment kinetics of the monocyte precursors and monocytes found in the BM after DT treatment of CD64[dtr] mice. Fig. S4 shows the lack of major impact of DT treatment on cDCs found in the skin of CD64[dtr] mice. Table S1, a separate Excel file, shows

the exhaustive lists of genes responsible for the IPA enrichments shown in Fig. 7 B.

References

Aoki, H., Y. Yamada, A. Hara, and T. Kunisada. 2009. Two distinct types of mouse melanocyte: Differential signaling requirement for the maintenance of non-cutaneous and dermal versus epidermal melanocytes. *Development.* 136:2511–2521. https://doi.org/10.1242/dev.037168

Autenrieth, S.E., P. Warnke, G.H. Wabnitz, C. Lucero Estrada, K.A. Pasquevich, D. Drechsler, M. Günter, K. Hochweller, A. Novakovic, S. Beer-Hammer, et al. 2012. Depletion of dendritic cells enhances innate anti-bacterial host defense through modulation of phagocyte homeostasis. *PLoS Pathog.* 8:e1002552. https://doi.org/10.1371/journal.ppat.1002552

Bain, C.C., C.L. Scott, H. Uronen-Hansson, S. Gudjonsson, O. Jansson, O. Grip, M. Guilliams, B. Malissen, W.W. Agace, and A.M. Mowat. 2013. Resident and pro-inflammatory macrophages in the colon represent alternative context-dependent fates of the same Ly6Chi monocyte precursors. *Mucosal Immunol.* 6:498–510. https://doi.org/10.1038/mi.2012.89

Bain, C.C., A. Bravo-Blas, C.L. Scott, E.G. Perdiguero, F. Geissmann, S. Henri, B. Malissen, L.C. Osborne, D. Artis, and A.M. Mowat. 2014. Constant replenishment from circulating monocytes maintains the macrophage pool in the intestine of adult mice. *Nat. Immunol.* 15:929–937. https://doi.org/10.1038/ni.2967

Bigley, V., M. Haniffa, S. Doulatov, X.N. Wang, R. Dickinson, N. McGovern, L. Jardine, S. Pagan, I. Dimmick, I. Chua, et al. 2011. The human syndrome

of dendritic cell, monocyte, B and NK lymphoid deficiency. *J. Exp. Med.* 208:227–234. https://doi.org/10.1084/jem.20101459

Bouladoux, N., C. Hennequin, C. Malosse, B. Malissen, Y. Belkaid, and S. Henri. 2017. Hapten-specific T cell-mediated skin inflammation: Flow cytometry analysis of mouse skin inflammatory infiltrate. *Methods Mol. Biol.* 1559:21–36. https://doi.org/10.1007/978-1-4939-6786-5_2

Brown, D.M., T.L. Fisher, C. Wei, J.G. Frelinger, and E.M. Lord. 2001. Tumours can act as adjuvants for humoral immunity. *Immunology.* 102:486–497. https://doi.org/10.1046/j.1365-2567.2001.01213.x

Carlin, L.M., E.G. Stamatiades, C. Auffray, R.N. Hanna, L. Glover, G. Viz-cay-Barrena, C.C. Hedrick, H.T. Cook, S. Diebold, and F. Geissmann. 2013. Nr4a1-dependent Ly6C(low) monocytes monitor endothelial cells and orchestrate their disposal. *Cell.* 153:362–375. https://doi.org/10.1016/j.cell.2013.03.010

De Trez, C., S. Magez, S. Akira, B. Ryffel, Y. Carlier, and E. Muraille. 2009. iNOS-producing inflammatory dendritic cells constitute the major infected cell type during the chronic Leishmania major infection phase of C57BL/6 resistant mice. *PLoS Pathog.* 5:e1000494. https://doi.org/10.1371/journal.ppat.1000494

Dhomen, N., J.S. Reis-Filho, S. da Rocha Dias, R. Hayward, K. Savage, V. Del-mas, L. Larue, C. Pritchard, and R. Marais. 2009. Oncogenic Braf induces melanocyte senescence and melanoma in mice. *Cancer Cell.* 15:294–303. https://doi.org/10.1016/j.ccr.2009.02.022

Duffield, J.S., S.J. Forbes, C.M. Constandinou, S. Clay, M. Partolina, S. Vuthoori, S. Wu, R. Lang, and J.P. Iredale. 2005. Selective depletion of macrophages reveals distinct, opposing roles during liver injury and repair. *J. Clin. Invest.* 115:56–65. https://doi.org/10.1172/JCI200522675

Durai, V., and K.M. Murphy. 2016. Functions of murine dendritic cells. *Immunity.* 45:719–736. https://doi.org/10.1016/j.immuni.2016.10.010

Elsaie, M.L., K. Nouri, V. Vejjabhinanta, M.P. Rivas, L.M. Villafradez-Diaz, A. Martins, and R. Rosso. 2009. Topical imiquimod in conjunction with Nd: YAG laser for tattoo removal. *Lasers Med. Sci.* 24:871–875. https://doi.org/10.1007/s10103-009-0709-9

Ferguson, J.E., S.M. Andrew, C.J. Jones, and P.J. August. 1997. The Q-switched neodymium:YAG laser and tattoos: A microscopic analysis of laser-tat-too interactions. *Br. J. Dermatol.* 137:405–410. https://doi.org/10.1111/j.1365-2133.1997.tb03747.x

Goudot, C., A. Coillard, A.C. Villani, P. Gueguen, A. Cros, S. Sarkizova, T.L. Tang-Huau, M. Bohec, S. Baulande, N. Hacohen, et al. 2017. Aryl hydro-carbon receptor controls monocyte differentiation into dendritic cells versus macrophages. *Immunity.* 47:582–596.e6. https://doi.org/10.1016/j.immuni.2017.08.016

Guilliams, M., C.A. Dutertre, C.L. Scott, N. McGovern, D. Sichien, S. Chakarov, S. Van Gassen, J. Chen, M. Poidinger, S. De Prijck, et al. 2016. Unsuper-vised high-dimensional analysis aligns dendritic cells across tissues and species. *Immunity.* 45:669–684. https://doi.org/10.1016/j.immuni.2016.08.015

Haniffa, M., F. Ginhoux, X.N. Wang, V. Bigley, M. Abel, I. Dimmick, S. Bullock, M. Grisotto, T. Booth, P. Taub, et al. 2009. Differential rates of replace-ment of human dermal dendritic cells and macrophages during hema-topoietic stem cell transplantation. *J. Exp. Med.* 206:371–385. https://doi.org/10.1084/jem.20081633

Haniffa, M., A. Shin, V. Bigley, N. McGovern, P. Teo, P. See, P.S. Wasan, X.N. Wang, F. Malinarich, B. Malleret, et al. 2012. Human tissues contain CD141hi cross-presenting dendritic cells with functional homology to mouse CD103+ nonlymphoid dendritic cells. *Immunity.* 37:60–73. https://doi.org/10.1016/j.immuni.2012.04.012

Hohl, T.M., A. Rivera, L. Lipuma, A. Gallegos, C. Shi, M. Mack, and E.G. Pamer. 2009. Inflammatory monocytes facilitate adaptive CD4 T cell responses during respiratory fungal infection. *Cell Host Microbe.* 6:470–481. https://doi.org/10.1016/j.chom.2009.10.007

Jakubzick, C., E.L. Gautier, S.L. Gibbings, D.K. Sojka, A. Schlitzer, T.E. Johnson, S. Ivanov, Q. Duan, S. Bala, T. Condon, et al. 2013. Minimal differentiation of classical monocytes as they survey steady-state tissues and transport antigen to lymph nodes. *Immunity.* 39:599–610. https://doi.org/10.1016/j.immuni.2013.08.007

Jung, S., J. Aliberti, P. Graemmel, M.J. Sunshine, G.W. Kreutzberg, A. Sher, and D.R. Littman. 2000. Analysis of fractalkine receptor CX(3)CR1 function by targeted deletion and green fluorescent protein reporter gene inser-tion. *Mol. Cell. Biol.* 20:4106–4114. https://doi.org/10.1128/MCB.20.11.4106-4114.2000

Madisen, L., T.A. Zwingman, S.M. Sunkin, S.W. Oh, H.A. Zariwala, H. Gu, L.L. Ng, R.D. Palmiter, M.J. Hawrylycz, A.R. Jones, et al. 2010. A robust and high-throughput Cre reporting and characterization system for the whole mouse brain. *Nat. Neurosci.* 13:133–140. https://doi.org/10.1038/nn.2467

Malissen, B., S. Tamoutounour, and S. Henri. 2014. The origins and functions of dendritic cells and macrophages in the skin. *Nat. Rev. Immunol.* 14:417–428. https://doi.org/10.1038/nri3683

McGovern, N., A. Schlitzer, M. Gunawan, L. Jardine, A. Shin, E. Poyner, K. Green, R. Dickinson, X.N. Wang, D. Low, et al. 2014. Human dermal CD14+ cells are a transient population of monocyte-derived macro-phages. *Immunity.* 41:465–477. https://doi.org/10.1016/j.immuni.2014.08.006

Mildner, A., J. Schonheit, A. Giladi, E. David, D. Lara-Astiaso, E. Lorenzo-Vivas, F. Paul, L. Chappell-Maor, J. Priller, A. Leutz, et al. 2017. Genomic char-acterization of murine monocytes reveals C/EBPβ transcription factor dependence of Ly6C⁻ cells. *Immunity.* 46:849–862.e7. https://doi.org/10.1016/j.immuni.2017.04.018

Pettitt, S.J., Q. Liang, X.Y. Rairdan, J.L. Moran, H.M. Prosser, D.R. Beier, K.C. Lloyd, A. Bradley, and W.C. Skarnes. 2009. Agouti C57BL/6N embryonic stem cells for mouse genetic resources. *Nat. Methods.* 6:493–495. https://doi.org/10.1038/nmeth.1342

Plantinga, M., M. Guilliams, M. Vanheerswynghels, K. Deswarte, F. Bran-co-Madeira, W. Toussaint, L. Vanhoutte, K. Neyt, N. Killeen, B. Malissen, et al. 2013. Conventional and monocyte-derived CD11b(+) dendritic cells initiate and maintain T helper 2 cell-mediated immunity to house dust mite allergen. *Immunity.* 38:322–335. https://doi.org/10.1016/j.immuni.2012.10.016

Salmon, H., J. Idoyaga, A. Rahman, M. Leboeuf, R. Remark, S. Jordan, M. Casanova-Acebes, M. Khudoynazarova, J. Agudo, N. Tung, et al. 2016. Expansion and activation of CD103(+) dendritic cell progenitors at the tumor site enhances tumor responses to therapeutic PD-L1 and BRAF inhibition. *Immunity.* 44:924–938. https://doi.org/10.1016/j.immuni.2016.03.012

Scott, C.L., F. Zheng, P. De Baetselier, L. Martens, Y. Saeys, S. De Prijck, S. Lip-pens, C. Abels, S. Schoonooghe, G. Raes, et al. 2016. Bone marrow-derived monocytes give rise to self-renewing and fully differentiated Kupffer cells. *Nat. Commun.* 7:10321. https://doi.org/10.1038/ncomms10321

Serbina, N.V., T.P. Salazar-Mather, C.A. Biron, W.A. Kuziel, and E.G. Pamer. 2003. TNF/iNOS-producing dendritic cells mediate innate immune defense against bacterial infection. *Immunity.* 19:59–70. https://doi.org/10.1016/S1074-7613(03)00171-7

Sheng, J., C. Ruedl, and K. Karjalainen. 2015. Most tissue-resident macro-phages except microglia are derived from fetal hematopoietic stem cells. *Immunity.* 43:382–393. https://doi.org/10.1016/j.immuni.2015.07.016

Slominski, A., J. Wortsman, P.M. Plonka, K.U. Schallreuter, R. Paus, and D.J. Tobin. 2005. Hair follicle pigmentation. *J. Invest. Dermatol.* 124:13–21. https://doi.org/10.1111/j.0022-202X.2004.23528.x

Sunderkötter, C., T. Nikolic, M.J. Dillon, N. Van Rooijen, M. Stehling, D.A. Drevets, and P.J. Leenen. 2004. Subpopulations of mouse blood mono-cytes differ in maturation stage and inflammatory response. *J. Immunol.* 172:4410–4417. https://doi.org/10.4049/jimmunol.172.7.4410

Tamoutounour, S., S. Henri, H. Lelouard, B. de Bovis, C. de Haar, C.J. van der Woude, A.M. Woltman, Y. Reyal, D. Bonnet, D. Sichien, et al. 2012. CD64 distinguishes macrophages from dendritic cells in the gut and reveals the Th1-inducing role of mesenteric lymph node macrophages during colitis. *Eur. J. Immunol.* 42:3150–3166. https://doi.org/10.1002/eji.201242847

Tamoutounour, S., M. Guilliams, F. Montanana Sanchis, H. Liu, D. Terhorst, C. Malosse, E. Pollet, L. Ardouin, H. Luche, C. Sanchez, et al. 2013. Origins and functional specialization of macrophages and of conventional and monocyte-derived dendritic cells in mouse skin. *Immunity.* 39:925–938. https://doi.org/10.1016/j.immuni.2013.10.004

Thomas, G.D., R.N. Hanna, N.T. Vasudevan, A.A. Hamers, C.E. Romanoski, S. McArdle, K.D. Ross, A. Blatchley, D. Yoakum, B.A. Hamilton, et al. 2016. Deleting an Nr4a1 super-enhancer subdomain ablates Ly6Clow mono-cytes while preserving macrophage gene function. *Immunity.* 45:975–987. https://doi.org/10.1016/j.immuni.2016.10.011

Tittel, A.P., C. Heuser, C. Ohliger, C. Llanto, S. Yona, G.J. Hämmerling, D.R. Engel, N. Garbi, and C. Kurts. 2012. Functionally relevant neutrophilia in CD11c diphtheria toxin receptor transgenic mice. *Nat. Methods.* 9:385–390. https://doi.org/10.1038/nmeth.1905

van Blijswijk, J., B.U. Schraml, N.C. Rogers, P.G. Whitney, S. Zelenay, S.E. Acton, and C. Reis e Sousa. 2015. Altered lymph node composition in diphtheria toxin receptor-based mouse models to ablate dendritic cells. *J. Immunol.* 194:307–315. https://doi.org/10.4049/jimmunol.1401999

van de Laar, L., W. Saelens, S. De Prijck, L. Martens, C.L. Scott, G. Van Isterdael, E. Hoffmann, R. Beyaert, Y. Saeys, B.N. Lambrecht, and M. Guilliams.

2016. Yolk sac macrophages, fetal liver, and adult monocytes can colonize an empty niche and develop into functional tissue-resident macrophages. *Immunity.* 44:755–768. https://doi.org/10.1016/j.immuni.2016 .02.017

Varol, C., L. Landsman, D.K. Fogg, L. Greenshtein, B. Gildor, R. Margalit, V. Kalchenko, F. Geissmann, and S. Jung. 2007. Monocytes give rise to mucosal, but not splenic, conventional dendritic cells. *J. Exp. Med.* 204:171–180. https://doi.org/10.1084/jem.20061011

Yona, S., K.W. Kim, Y. Wolf, A. Mildner, D. Varol, M. Breker, D. Strauss-Ayali, S. Viukov, M. Guilliams, A. Misharin, et al. 2013. Fate mapping reveals origins and dynamics of monocytes and tissue macrophages under homeostasis. *Immunity.* 38:79–91. https://doi.org/10.1016/j.immuni .2012.12.001

Yu, W., J. Chen, Y. Xiong, F.J. Pixley, Y.G. Yeung, and E.R. Stanley. 2012. Macrophage proliferation is regulated through CSF-1 receptor tyrosines 544, 559, and 807. *J. Biol. Chem.* 287:13694–13704. https://doi.org/10.1074/jbc .M112.355610

Zaba, L.C., J. Fuentes-Duculan, R.M. Steinman, J.G. Krueger, and M.A. Lowes. 2007. Normal human dermis contains distinct populations of CD11c+B-DCA-1+ dendritic cells and CD163+FXIIIA+ macrophages. *J. Clin. Invest.* 117:2517–2525. https://doi.org/10.1172/JCI32282

Zelenay, S., A.G. van der Veen, J.P. Böttcher, K.J. Snelgrove, N. Rogers, S.E. Acton, P. Chakravarty, M.R. Girotti, R. Marais, S.A. Quezada, et al. 2015. Cyclooxygenase-dependent tumor growth through evasion of immunity. *Cell.* 162:1257–1270. https://doi.org/10.1016/j.cell.2015.08.015